Chapter 3

Heterogeneous base catalyst derived from *Musa champa* plant for production of biodiesel

3.1 Introduction

"*Musa champa* Hort. ex Hook. F. (AB) is a variety of bananas belonging to Musaceae family and is known as Chinichampa in local languages in the state of Assam, India. *M. champa* is a distinct banana that has small-sized fruit (6–9 cm), and a thin and dark green peel that turns to golden yellow color when fully ripened. It bears a dark red flower; its flavor is a little bit sour and pleasant sweetness (sugar taste) having a good banana aroma. This cultivar is the hardest in the medium-tall grown (3–4 m). Depending on the fertility of the soil and region, it bears fruit with 150–250 fingers fruit and weighs about 10–16 kg in a bunch (Goswami and Handique, 2013; Swain et al., 2016). Very recently, a synthetic green catalyst from the *M. champa* peel was developed and reported its efficient utilization in the Claisen–Schmidt reaction for the synthesis of chalcone and flavone derivatives (Tamuli et al., 2020). However, to date, the application of derived catalysts from the peel, stem, and rhizome of *M. champa* in transesterification reactions for the production of biodiesel has not been reported in any scientific papers to the best of our knowledge. In this study, it was presumed that the post-harvest *M. champa* plant derived material, which is renewable, available in abundant quantity, low-cost, and eco-friendly, would be utilized as an effective solid catalyst for the easy synthesis of biodiesel. Thus, the purpose of the present work was to prepare a heterogeneous ash-based catalyst from the post-harvest *M. champa* plant and to utilize the derived materials in *Jatropha curcas* oil-based biodiesel production. This paper reported the comparative catalytic efficacy studies of the catalysts prepared from the peel, stem, and rhizome parts of *M. champa* in biodiesel production from *J. curcas* oil, and the biodiesel characterization, fuel properties and successful analysis of the catalysts (Basumatary et al., 2023). This study also discussed the outcomes of the experiments carried out in optimizing the reaction parameters such as MTOMR (methanol to oil molar ratio), reaction temperature, and effects of catalyst dosage loaded in wt.% along with the catalyst reusability at ORCs (optimum reaction conditions), and activation energy of the reaction.

3.2 Experimental Methods

3.2.1. Chemicals and materials

The chemicals with its brand utilized in this work are similar with the previous study (**Chapter 2**) which are mentioned in the **Section 2.2.1** (**Page no. 34**). For the preparation of the catalyst, the fruit's peel, stem, and rhizome of *M. champa* were collected from Debargaon, Kokrajhar, India. The *Jatropha curcas* oil used in this study was purchased online from IndiaMART.

3.2.2 Methods

3.2.2.1 Preparation of the catalysts

The collected *M. champa* fruit's peel, stem and rhizome were washed with water to remove adhered mud sand and other impurities. The washed parts of the peel, stem and rhizome were separately cut into small and thin pieces. They were sliced into such sizes that they could be dried and burnt easily and quickly as shown in (**Fig. 3.1**). Sliced pieces were sun-dried for 10–12 days. The further steps of preparation were followed as mentioned in Chapter **2 (Section 2.2.2.1, Page no. 34**). In this study, the abbreviations used for naming the prepared catalysts are (a) BMCP (burnt *Musa champa* peel) catalyst, (b) BMCS (burnt *Musa champa* stem) catalyst, (c) BMCR (burnt *Musa champa* rhizome) catalyst, (d) CMCP-550 (calcined *Musa champa* peel) catalyst, (e) CMCS-550 (calcined *Musa champa* stem) catalyst, and (f) CMCR-550 (calcined *Musa champa* rhizome) catalyst.

Fig. 3.1. *M. champa* peel (A–C), stem (D–F) and rhizome (G–I) dried materials for catalyst preparation.

3.2.2.2 Characterization of the catalysts

Thermogravimetric analysis (TGA) was performed to determine the weight loss percentage and the thermal stability of the burnt ash (uncalcined) *M. champa* catalysts using a thermogravimetric analyzer (Make: TA, Model: SDTQ600, USA) employing heating at a constant rate of 10 ^{o}C/min up to 600 ^{o}C with a constant flow of N_2 gas. Powder XRD (ULTIMA IV, Rigaku) analysis was conducted to investigate the crystalline compounds present in the catalyst. The FT-IR, BET, XPS, FESEM and EDX analyses were carried out by the same instrument and following the same procedure as mentioned in Chapter **2 (Section 2.2.2.2, Page no. 35-36**). The crystalline structures of the catalysts were investigated from HRTEM images and SAED patterns recorded using JEM-2100JEOL instrument (200 kV). The determination of soluble alkalinity, pH value and the basicity of the *M. champa* catalysts were estimated as per the procedure mentioned in previous Chapter **2 (Section 2.2.2.2, Page no. 36**).

3.2.2.3 Biodiesel preparation, characterization and property determination

In this study, three different calcined catalysts (CMCP-550, CMCS-550 and CMCR-550) and burnt *M. champa* catalysts (BMCP, BMCS and BMCR) were investigated for the transesterification of *J. curcas* oil. The biodiesel preparation via transesterification reaction and investigation of optimum reaction conditions (ORCs) was carried out by following similar procedure mentioned in **Chapter 2 (Section 2.2.2.3, Page no. 36-37**). Similarly, the same equation **2.1** in **Chapter 2 (Section 2.2.2.3, Page no. 37**) was applied to calculate the yield % of the biodiesel.

^{1}H NMR analyses of *J. curcas* oil and synthesized biodiesel were recorded with Bruker FT-NMR Spectrometer (Avance II) using $CDCl_3$ solvent at 400 MHz. To investigate the changes in stretching and bending vibrations of the functional groups of oil to biodiesel, FT-IR spectra were recorded on a Shimadzu FT-IR spectrometer (Miracle 10, 00644). The methyl esters compositions of biodiesel were determined using a Perkin Elmer GC-MS, 193 Claurus 680 Gas Chromatograph/Claurus 600 GC Mass spectrometer. For this analysis, the starting temperature was kept at 60 °C for 6 min. After that, at the rate of 5 °C/min, it was raised to 180 °C, and then increased to 280 °C at the rate of 10 °C/min. Once the temperature was maintained at 250 °C, the sample was placed and run. It was examined with TurboMass Ver5.4.2 software. Helium was used as carrier gas which split in the ratio of 20:1 at a flow rate of 1 mL/min, the mass scan was ranging from 50 to 500 Da and GC column was Elite 35 MS with 60.0 m × 250 m dimensions. The transfer temperature was 180 °C and that of the source temperature was 160 °C. The physicochemical properties of the synthesized biodiesel from *J. curcas* oil were tested with the similar protocol as mentioned in **Chapter 2 (Section 2.2.2.3, Page no. 37-38**). Additionally, acid value (AV) of oil and biodiesel were also evaluated as prescribed by Barua et al. (2014). The amount of free fatty acid (FFA) was also determined from the AV (FFA = AV/2).

3.3 Results and Discussion

3.3.1 Characterization of catalysts

3.3.1.1 Thermogravimetric analysis

Thermogravimetric (TGA) analyses of burnt *M. champa* catalysts were examined and the thermograms are shown in **Fig. 3.2**. The analyses displayed almost similar TGA patterns for BMCP, BMCS and BMCR catalysts. During the heat treatment, the gradual weight losses were indicated in the thermograms at three phases. Initially, the heating till about 180 ^{o}C, the weight loss may be due to the release of moisture adsorbed on the catalyst's surface. In the second

phase, the materials were found to be moderately stable as no sharp changes were observed between the temperature range of 180 °C to till about 450 °C, where chemical decomposition may not occur. However, this may be attributed due to the loss of water of crystallization present in the materials. Thereafter, heating the material beyond the temperature of 450 °C, sharp weight loss was observed. On further calcination at a much higher temperature, i.e., beyond 450 °C, the decomposition of the carbonaceous materials can be expected which may be associated with the release of CO_2 and CO (Nath et al., 2020; Sharma et al., 2012), and more specifically, the decomposition of metal carbonates present in the material may initiate from this temperature.

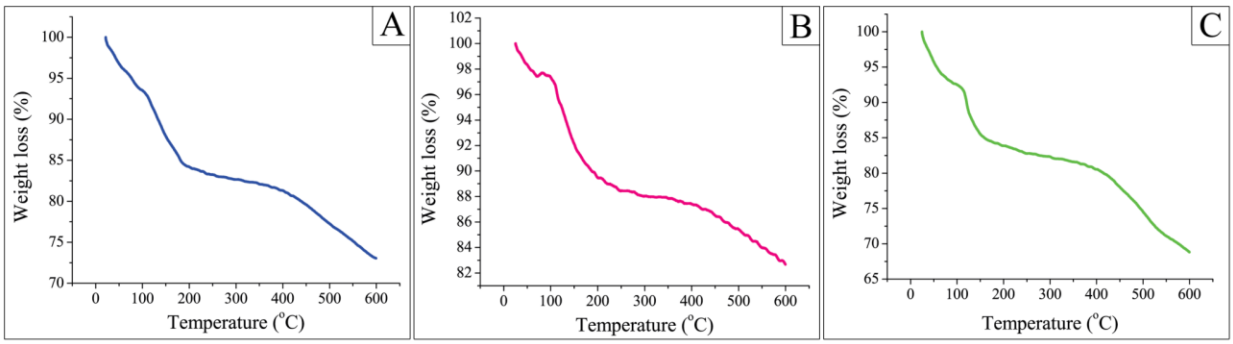

Fig. 3.2. TGA thermograms of BMCP (A), BMCS (B) and BMCR (C) catalysts.

3.3.1.2 XRD analyses of *M. champa* catalysts

The *M. champa* peel, stem and rhizome catalysts calcined at 550 °C were characterized by powder XRD (**Fig. 3.3**) to examine the crystalline compounds present in the catalysts. The XRD data obtained were compared with the database of 2θ values of JCPDS (ICDD 2003) and reported data of plant-based catalysts. From the XRD pattern of *M. champa* peel catalyst (**Fig. 3.3**), the abundance of K_2CO_3 was noted from the 2θ values (degree) at 26.72, 29.58, 32.11, 34.40, 41.21 and 43.25. The KCl noticed was characterized by the 2θ values at 28.28, 40.46, 50.15 and 72.97. The presence of K_2O was established by 2θ values at 39.76 and 48.35. The existence of $CaCO_3$ was indicated by a 2θ value of 38.43. The peak at 2θ values of 32.54 and 66.32 represented CaO in the catalysts. The presence of SiO_2 in *M. champa* peel catalyst was identified by a peak that appeared at a 2θ value of 25.72. Collectively, the components present in *M. champa* peel catalyst were K_2CO_3, KCl, K_2O, $CaCO_3$, CaO and SiO_2. In this study, the XRD pattern for *M. champa* stem (**Fig. 3.3**) exhibited characteristic peaks at 2θ of 29.76, 30.53, 33.92, 40.70, 41.79 and 43.06 which are attributed to the presence of K_2CO_3. The peaks obtained at 2θ of 28.11, 39.54, 50.13 and 73.97 referred to the existence of KCl. The presence

of K_2O was recognized by the peaks at 2θ value of 48.37. The other inorganic components of Ca in *M. champa* stem such as $CaCO_3$, CaO and $CaMg(CO_3)_2$ were revealed by the peaks at 2θ = 33.25 ($CaCO_3$), 2θ= 32.52,66.52 (CaO), and 2θ= 45.01 for $CaMg(CO_3)_2$. The peak at 2θ value of 28.52 was identified as SrO. The presence of Fe_2O_3 in *M. champa* stem was also obtained at the 2θ values of 23.83 and 32.75. Therefore, altogether the identified components in *M. champa* stem catalyst were K_2CO_3, KCl, K_2O, $CaCO_3$, CaO, $CaMg(CO_3)_2$, SrO and Fe_2O_3. Like the peel and stem catalysts, **Fig. 3.3** portrayed that the calcined *M. champa* rhizome catalyst also comprised a similar type of crystalline components with comparable 2θ data. These XRD analyses depicted the existence of K as K_2CO_3, K_2O and KCl along with other metal oxides and carbonates, and it was expected that the metal oxides and carbonates are contributing to the catalyzed biodiesel synthesis of this study. Gohain et al. (2017) performed the XRD analysis for *M. balbisiana* peel catalyst and reported the presence of potassium and calcium carbonates and oxides as dominant species. The XRD analyses reports of this study are in good agreement with the reported catalysts from waste banana peel (Fan et al., 2019), *Sesamum indicum* (Nath et al., 2020), *Musa acuminata* peduncle (Balajii and Niju, 2019), tucumã peel (Mendonça et al., 2019b), orange peel (Changmai et al., 2020a) and pawpaw peel (Oladipo et al., 2020).

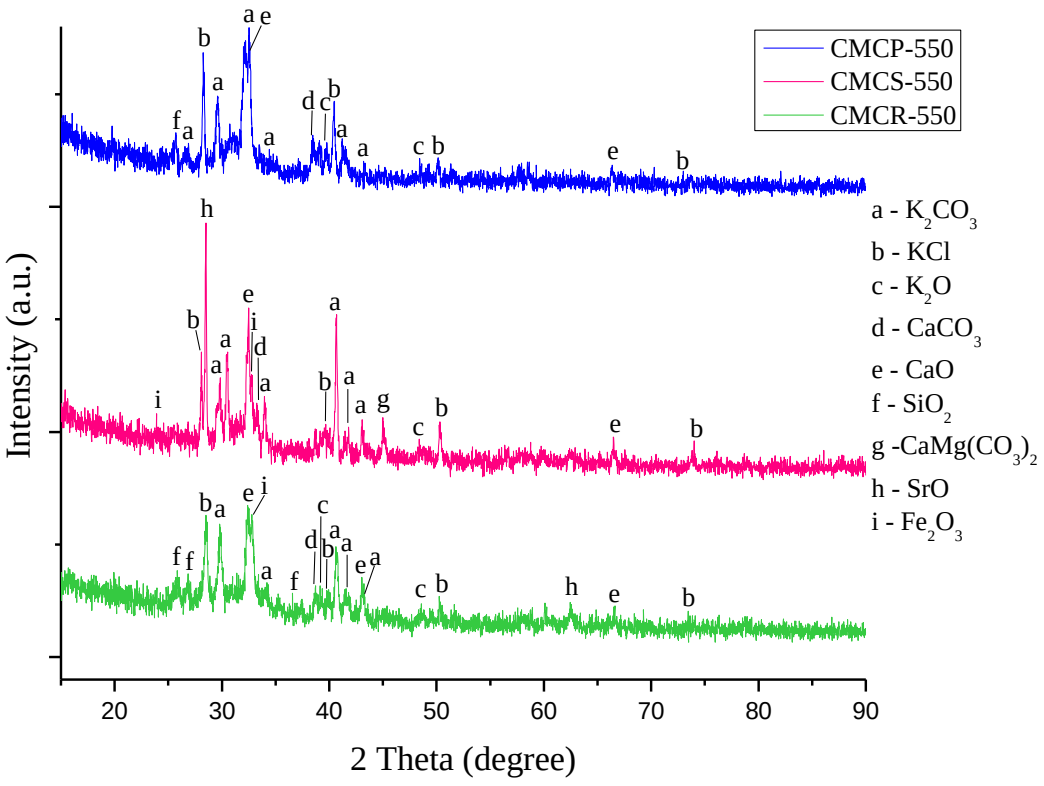

Fig. 3.3. XRD patterns of calcined *M. champa* catalysts.

3.3.1.3 FT-IR studies

The FT-IR studies of CMCP-550, CMCS-550, CMCR-550 and the 3rd recycled catalysts are presented in **Fig. 3.4**. The appearance of signals for CMCP-550 at 3490 cm^{-1}, 3rd recycled catalyst (CMCP-550) at 3435 cm^{-1}, CMCS-550 at 3441 cm^{-1} and for CMCR-550 catalyst at 3421 cm^{-1} are assigned to O-H stretching vibrations indicating the adsorption of moisture on the surface of the catalysts (Tamuli et al., 2020; Changmai et al., 2021). The various peaks for the catalyst CMCP-550 at 1641, 1462, 1389, 1090 cm^{-1}, 3rd recycled (CMCP-550) at 1641, 1469, 1419, 1124, 1056 cm^{-1}, CMCS-550 at 1641, 1462, 1403, 1049 cm^{-1} and for CMCR-550 catalyst at 1641, 1536, 1403, 1097 cm^{-1} were observed. These absorption bands noticed between the ranges of 1641-1049 cm^{-1} are attributed to the bending and stretching vibrations of C-O bond of carbonate ions (CO_3^{2-} group), indicating the presence of K, Ca and other metal carbonates in the catalysts (Pathak et al., 2018; Gohain et al., 2020a). The existence of K_2CO_3 and $CaCO_3$ is also described in the XRD studies (**Fig. 3.3**). The Si-O-Si bond vibrations of SiO_2 in the catalysts were observed for CMCP-550 at 859 cm^{-1}, 3rd recycled (CMCP-550) at 886 cm^{-1}, CMCS-550 at 866 cm^{-1} and for CMCR-550 at 866 and 761cm^{-1} (Etim et al., 2021; Tamuli et al., 2020). The occurrence of peaks at 682, 614, 688, and 675 cm^{-1} are responsible for the existence of K_2O, CaO and other metal oxides due to the bending and stretching vibrations of metal oxides. Similar results were also described in the studies of Etim et al. (2021) and Falowo and Betiku (2022). The data of FT-IR characterization for present catalysts affirms that the catalysts consist of metal carbonates and metal oxides specifically K_2CO_3, $CaCO_3$, K_2O, CaO and SiO_2 which are in accordance with the analyzed XRD results (**Fig. 3.3**) of this work.

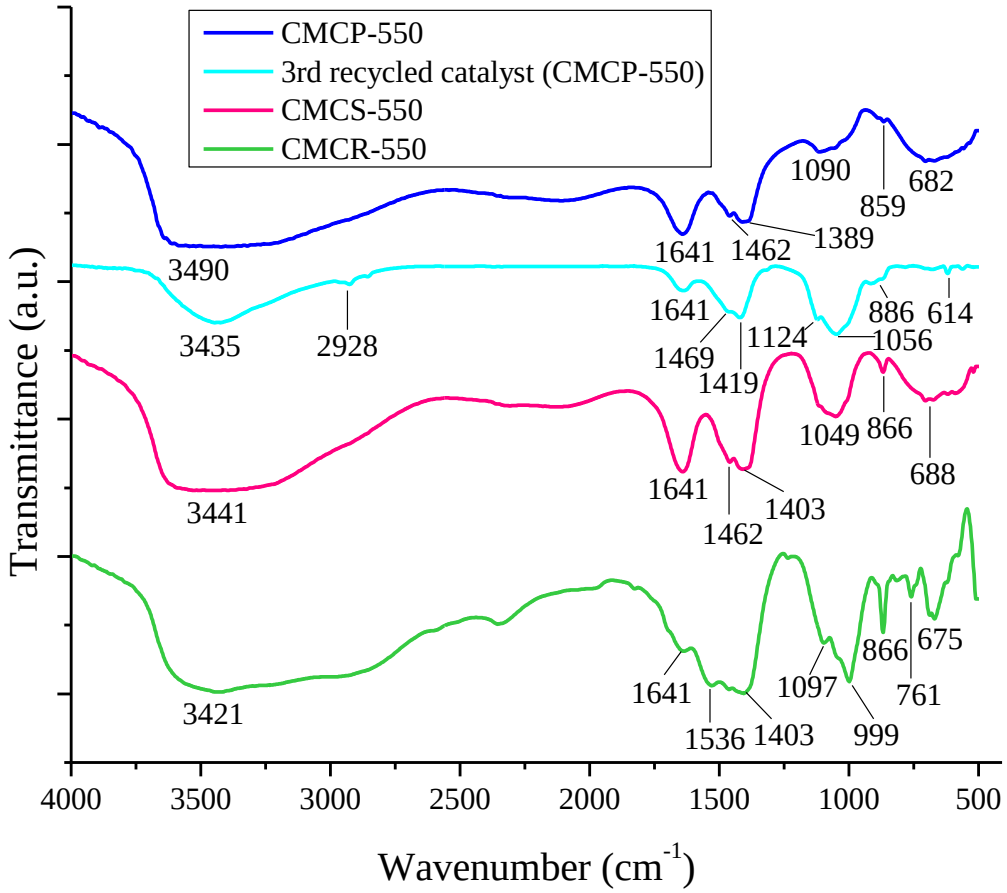

Fig. 3.4. FT-IR spectra of calcined *M. champa* catalysts.

3.3.1.4 BET studies

The surface areas of CMCP-550, CMCS-550 and CMCR-550 catalysts were determined by the BET technique (**Table 3.1**) and found to be 6.848, 1.388 and 0.876 $m^2 g^{-1}$ respectively. The observed surface area values were found to be relatively lower than other reported data of biomass catalysts such as *Lemna perpusilla* (9.6 $m^2 g^{-1}$) (Chouhan and Sarma, 2013), waste snail shell (7.0 $m^2 g^{-1}$) (Laskar et al., 2018), *Musa balbisiana* Colla peel (14.0 $m^2 g^{-1}$) (Gohain et al., 2017). However, lower surface areas than CMCP-550 catalyst were reported in tucumã peel (1.0 $m^2 g^{-1}$) by Mendonça et al. (2019b) and *Musa balbisiana* underground stem (0.04 $m^2 g^{-1}$) by Kumar et al. (2016). The cause for the lower surface area may be due to the presence of less amount of unburnt-carbon particles in the prepared catalysts (Pathak et al., 2018). Comparatively, the CMCP-550 catalyst showed a greater surface area than CMCS-550 and CMCR-550 catalysts which supported the higher catalytic performance of the CMCP-550 catalyst. The pore volumes of CMCP-550, CMCS-550 and CMCR-550 catalysts were found to be 0.018, 0.004 and 0.003 $cm^3 g^{-1}$ and the respective pore diameters were 2.327, 2.246 and

2.587 nm (**Fig. 3.5**, **Table 3.1**). **Fig. 3.5** (A–C) are the N_2 adsorption-desorption isotherms of the calcined catalysts and are found as per the classification of Brunauer-Deming-Deming-Teller (BDDT) method (Tian et al., 2020; Zhang et al., 2019). From **Fig. 3.5**, the plots of all three catalysts are characterized as type IV isotherm and H3 hysteresis loop. In agreement with the physisorption perspectives, the porosity nature of CMCP-550 catalyst is found to be a micro-mesoporous structure as its pore size is within 1.8–12.06 nm. The pore sizes of CMCS-550 and CMCR-550 catalysts are ranging from 2.2–20 nm and 2.13–16.12 nm, respectively, which indicates that these catalysts are comprised of the mesoporous structure.

Table 3.1: Surface area, pore volume and pore diameter of calcined *M. champa* catalyst.

Calcined catalyst	**Surface area ($m^2 g^{-1}$)**	**Pore volume ($cm^3 g^{-1}$)**	**Pore diameter (nm)**
CMCP-550	6.848	0.018	2.327
CMCS-550	1.388	0.004	2.246
CMCR-550	0.876	0.003	2.587

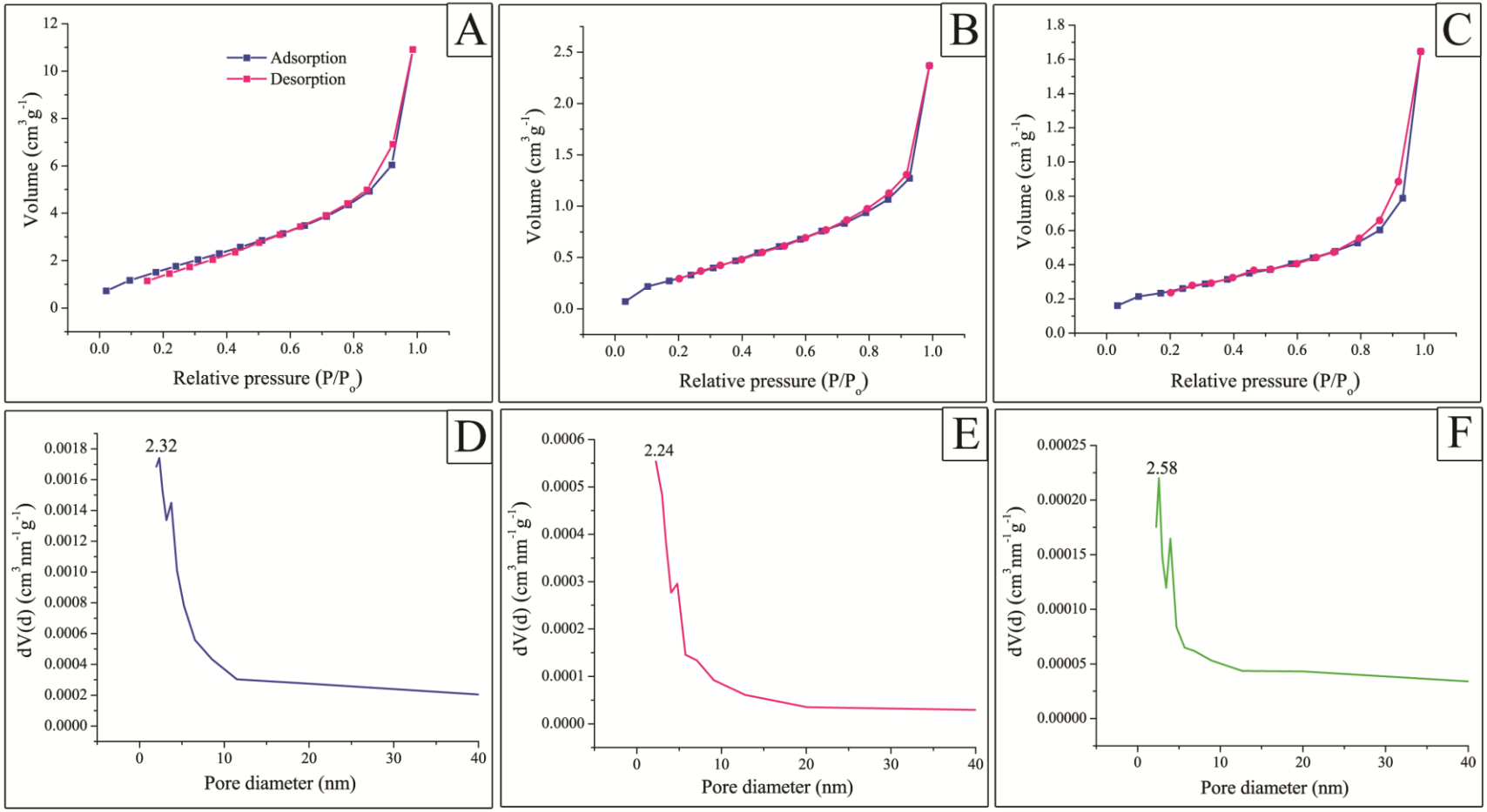

Fig. 3.5. N_2 adsorption-desorption isotherms (A–C) and adsorption pore size distribution of CMCP-550 (D), CMCS-550 (E) and CMCR-550 (F) catalysts**.**

3.3.1.5 FESEM studies

The FESEM images of BMCP, BMCS and BMCR catalysts showing different morphologies are displayed in **Fig. 3.6**. In BMCP catalyst (**Fig. 3.6** A), long cylindrical shaped and many irregulars and non-uniform polygon-like agglomerated particles were observed. In the BMCS catalyst (**Fig. 3.6** C), the distinct clusters of hexagonal, cuboidal and pentagonal shapes were observed. The image of the BMCR catalyst (**Fig. 3.6** E) viewed at 2 μm exhibited different morphological structures representing an irregular surface with bitty and non-uniform polygon-like cluster particles. The FESEM images of the calcined catalysts at 1 μm magnification are shown in **Fig. 3.7** exhibiting changes in the morphologies on calcination of the catalysts at 550 ^{o}C. The morphological characteristic of CMCP-550 catalyst (**Fig. 3.7** A) indicated microporous, clusters of oval-like shape, spongy and more agglomeration than the burnt ash catalyst (**Fig. 3.6** A). **Fig. 3.7** C demonstrated that CMCS-550 catalyst was spongy and asymmetrical with rough surfaces. CMCR-550 catalyst exhibited rough textural sintered ash having a lump shape on the surface as shown in **Fig. 3.7** E. The morphological structures of the 3rd recycled catalyst are illustrated in **Fig. 3.8**, where light-tiny packed fragmented needle-like strips and clustered particles are observed.

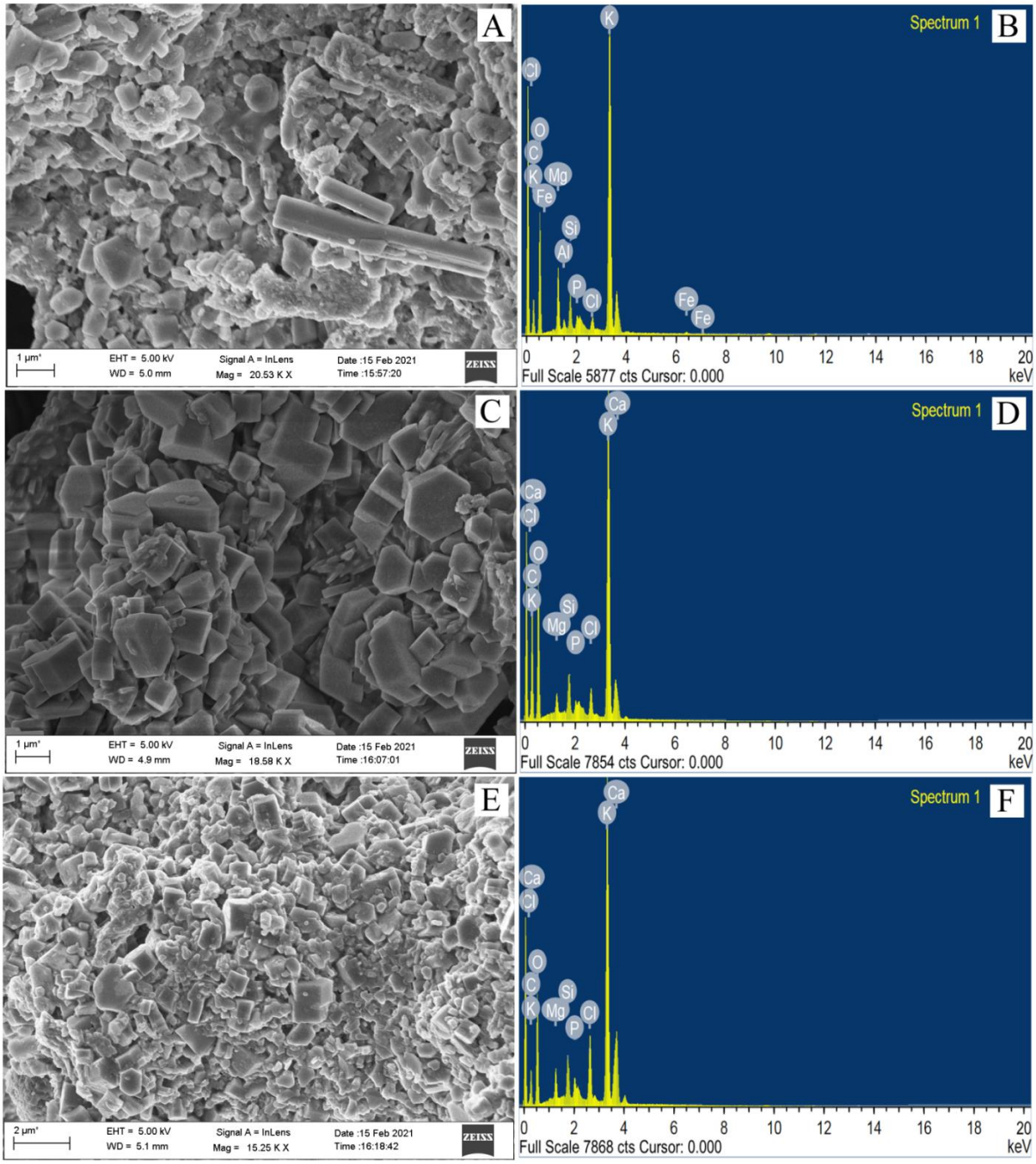

Fig. 3.6. FESEM images (A, C, E) and EDX spectra (B, D, F) of BMCP peel (A, B), BMCS (C, D) and BMCR (E, F) catalysts.

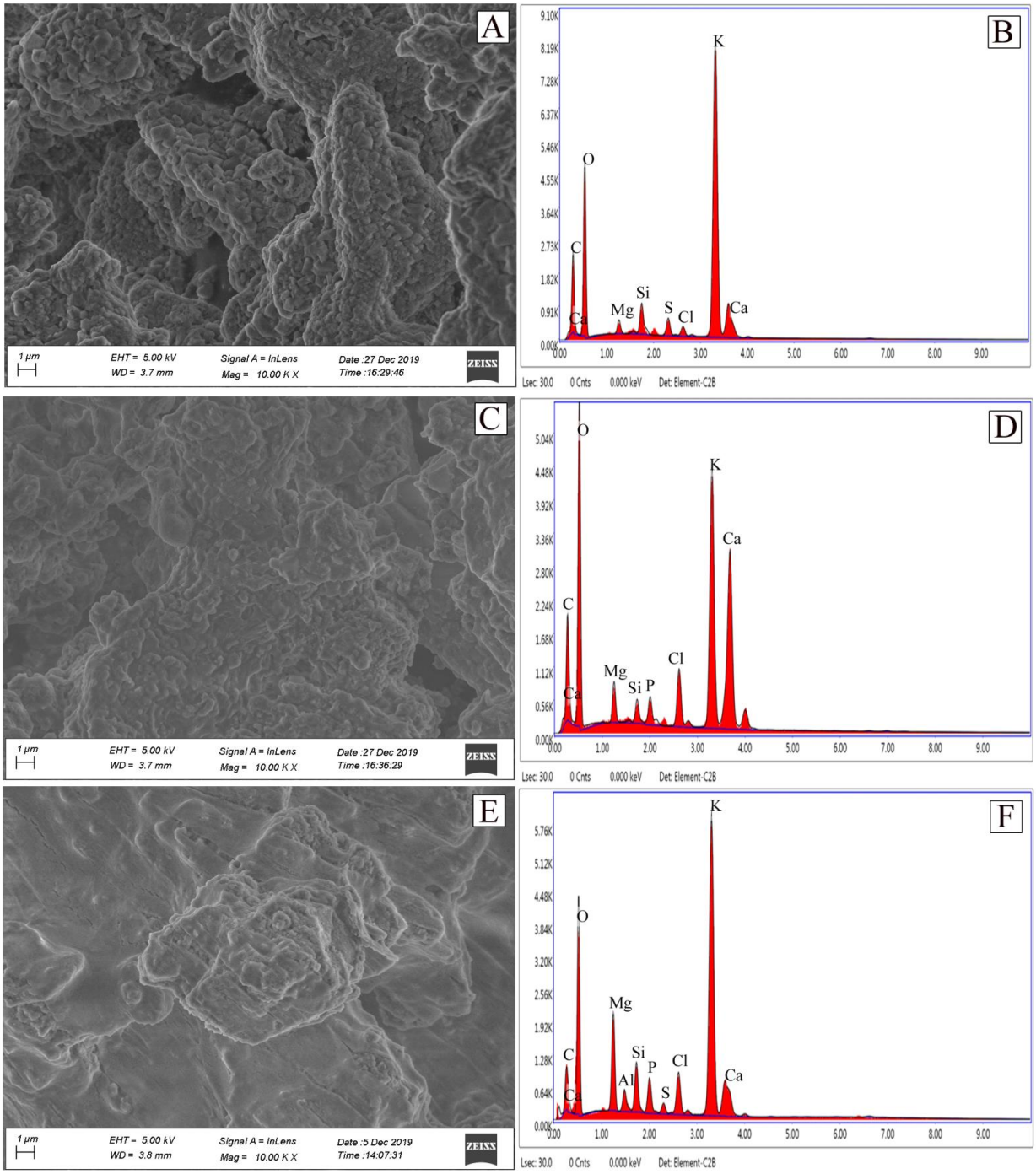

Fig. 3.7. FESEM images (A, C, E) and EDX spectra (B, D, F) of CMCP-550 (A, B), CMCS-550 (C, D) and CMCR-550 (E, F) catalysts.

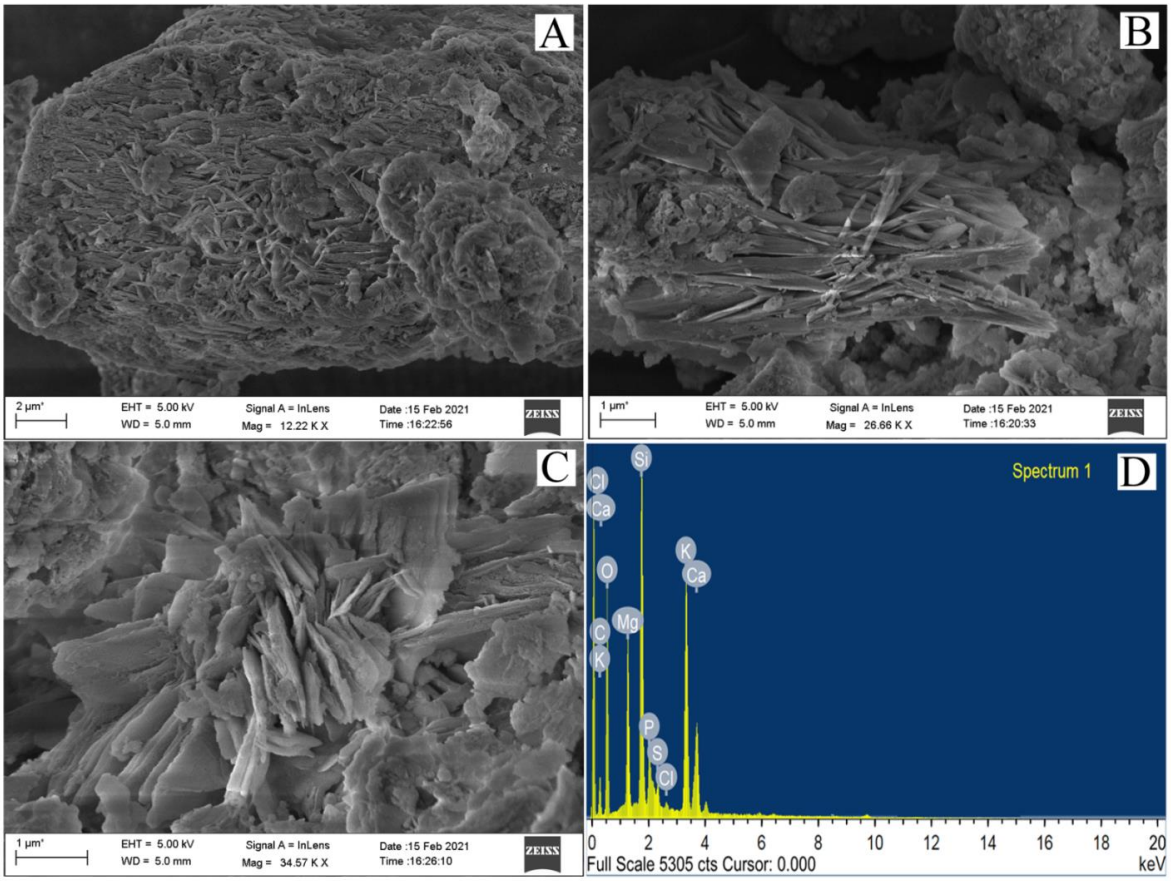

Fig. 3.8. FESEM images (A–C) and EDX spectrum (D) of 3rd recycled catalyst of calcined *M. champa* peel (CMCP-550).

3.3.1.6 EDX studies

The composition of the elements found in burnt ash and calcined *M. champa* catalysts along with the recycled catalyst studied from the EDX technique (**Fig. 3.6-3.8**) is summarized in **Table 3.2** and **Table 3.3** respectively. It is remarkable to mention that the catalysts of the present study consist of C, O, and K as major elements, and Mg, Si, Cl, Ca, P, Al, and Fe are present as minor elements. The weight % of K present in BMCP catalyst was (27.88 %), BMCS (19.55 %) and BMCR (23.62 %). However, K content in CMCP-550 catalyst was 47.49 % followed by CMCR-550 (40.94 %) and CMCS-550 (24.09 %) and, a low amount of K was detected in the 3rd recycled catalyst (11.37 %) (**Table 3.3**). The amount of C present in BMCP was 14.17 %, BMCS was 29.78 %, BMCR was 16.88 % and in the 3rd recycled CMCP-550 catalyst, it was 18.94 %. Comparatively lower C content was found in CMCP-550 (6.78 %), CMCS-550 (4.94 %), CMCR-550 (0.70 %). The high weight % of oxygen contents were observed both in burnt ash and calcined catalysts (**Table 3.2, Table 3.3**). From EDX analyses, it was observed that a higher amount of K was present in the calcined catalysts than the burnt

ash catalysts of this study, the highest being in CMCP-550 catalyst which exhibited better catalytic efficacy. The presence of oxygen and carbon indicated that the present catalysts mainly contained metal carbonates and oxides which are also supported by XRD (**Fig. 3.3**) and FTIR (**Fig. 3.4**) analyses. The catalysts with high contents of K that showed good activity were *Sesamum indicum* (Nath et al., 2020), *Musa acuminata* peel (Pathak et al., 2018), and *Musa acuminata* peduncle (Balaji and Niju, 2019). The elemental components of the calcined *M. champa* were compared with other reported solid catalysts derived from different waste biomasses (Nath et al., 2019; Aleman-Ramirez et al., 2021; Etim et al., 2018; Niju et al., 2021; Li et al., 2018), that were utilized in the production of biodiesel which are summarized in **Table 3.4**. It can be noticed that the catalysts made from different waste biomasses have different concentrations of chemical elements and the most of the catalysts exhibited higher concentrations of K compared to other metals. The variation of chemical contents depends upon various factors like soil character, climate, environmental conditions, geographical location and plant age in addition to calcination temperature and method of catalyst preparation. It is also remarkable to mention that the calcination temperature of such catalysts and concentration of metals like K in the form of its carbonate and oxide are mainly responsible for exhibiting good catalytic activities in biodiesel production.

Table 3.2: FESEM-EDX analyses of burnt *M. Champa* materials.

Elements	**Composition of burnt *M. champa* materials**					
	BMCP		**BMCS**		**BMCR**	
	Weight %	**Atomic %**	**Weight %**	**Atomic %**	**Weight %**	**Atomic %**
C	14.17	22.38	29.78	41.63	16.80	26.85
O	48.68	57.71	44.48	46.66	43.76	52.49
Mg	4.38	3.41	0.94	0.66	1.83	1.44
Si	2.09	1.41	1.82	1.09	2.38	1.62
Cl	0.96	0.52	1.46	0.69	4.15	2.25
K	27.88	13.53	19.55	8.38	23.62	11.59
Ca	-	-	1.45	0.61	6.17	2.95
P	0.74	0.45	0.48	0.26	1.25	0.78

Al	0.56	0.40	-	-	-	-
Fe	0.51	0.17	-	-	-	-

Table 3.3: FESEM-EDX analyses of calcined *M. champa* catalysts.

Elements	**Composition of *M. champa* catalyst calcined at 550 ^{o}C**							
	CMCP-550		**3rd recycled catalyst (CMCP-550)**		**CMCS-550**		**CMCR-550**	
	Weight %	**Atomic %**	**Weight %**	**Atomic %**	**Weight %**	**Atomic %**	**Weight %**	**Atomic %**
C	6.78	12.88	18.94	28.64	4.94	9.34	0.70	1.42
O	37.55	53.56	44.22	50.22	41.07	58.29	36.22	55.12
Mg	1.01	0.95	5.90	4.40	1.86	1.74	6.26	6.27
Si	2.05	1.67	10.88	7.04	0.93	0.75	2.84	2.46
S	1.63	1.16	1.00	0.57	-	-	0.84	0.64
Cl	1.09	0.70	0.33	0.17	3.79	2.43	4.04	2.78
K	47.49	27.72	11.37	5.28	24.09	13.99	40.94	25.50
Ca	2.40	1.37	4.83	2.18	21.88	12.40	4.14	2.52
P	-	-	2.50	1.46	1.44	1.06	2.72	2.14
Al	-	-	-	-	-	-	1.28	1.16

Table 3.4: Comparison of composition of *M. champa* catalyst with other reported solid catalysts derived from waste biomasses.

Source of catalyst	Calcination condition	Composition (%)													
		Na	**K**	**Ca**	**Mg**	**Al**	**Si**	**P**	**Cl**	**Fe**	**Mn**	**Zn**	**Sr**	**C**	**O**
Musa champa peel (This work)	550 ^{o}C, 2 h	-	47.49	2.40	1.01	-	2.05	-	1.09	-	-	-	-	6.78	37.55
Sesamum indicum (Nath et al., 2020)	550 ^{o}C, 2 h	1.42	29.64	33.80	9.68	–	11.32	–	–	1.70	0.80	0.54	11.09	–	–
Acacia nilotica stem (Sharma et al., 2012)	500 ^{o}C, 3 h	0.6	6.7	13.3	2.7	8.3	15.7	0.80	–	–	–	–	–	–	–
Lemna perpusilla (Chouhan and Sarma, 2013)	550 ^{o}C, 2 h	0.53	11.32	–	–	–	82.51	–	–	–	–	–	–	5.10	–
Pawpaw peel (Oladipo et al., 2020)	600 ^{o}C, 4 h	0.00	23.89	2.86	1.00	-	0.00	3.04	0.87	0.00	-	-	-	29.16	36.72

Brassica nigra (Nath et al., 2019)	550 °C, 2 h	0.94	56.13	26.04	2.86	–	5.37	–	–	1.26	0.05	1.63	5.72	–	–
Moringa leaves (Aleman-Ramirez et al., 2021)	500 °C, 2 h	–	9.87	10.09	5.92	–	–	1.19	–	–	–	–	–	12.19	59.57
Musa paradisiacal peel (Etim et al., 2018)	700 °C, 4 h	–	51.02	–	1.15	0.29	2.51	1.84	6.27	–	–	–	–	–	36.43
Poovan banana pseudostem (Niju et al., 2021)	700 °C, 4 h	0.4	20.2	7.4	4.52	0.25	3.79	1.91	8.99	0.51	–	–	–	–	–
Camphor leaf (Li et al., 2018)	800 °C, 2 h	0.23	1.22	12.05	1.82	2.70	–	–	–	–	–	–	–	–	–

Musa balbisiana underground stem (Sarma et al., 2014)	550 °C, 2 h	0.61 (Na_2O)	25.09 (K_2O)	10.44 (CaO)	10.04 (MgO)	4.07 (Al_2O_3)	35.92 (SiO_2)	4.47 (P_2O_5)	–	1.88 (Fe_2O_3)	–	–	1.89 (SrO)	–	–
Carica papaya peel (Etim et al., 2021)	700 °C, 4 h	0.82	36.74	3.64	1.16	-	0.71	4.22	10.3	-	-	-	-	-	44.1
Carica papaya stem (Gohain et al., 2020a)	700 °C, 4 h	14.78	56.71	21.08	4.41	–	3.02	–	–	–	–	–	–	–	–
Heteropanax fragrans (Basumatary et al., 2021c)	550 °C, 2 h	-	19.05	5.13	0.86	0.44	8.51	0.64	1.92	-	-	-	-	16.71	46.74
Musa balbisiana peel (Gohain et al., 2017)	700 °C, 4 h	10.41	41.37	36.08	12.02	–	–	–	–	–	–	–	–	–	–

Musa acuminata peduncle (Balajii and Niju, 2019)	700 °C, 4 h	–	42.23	1.70	1.39	–	1.54	1.91	–	–	–	–	–	–	50.54
Musa spp peduncle (Balajii and Niju, 2020)	700 °C, 4 h	–	52.04	5.27	5.71	–	–	–	–	–	–	–	–	–	36.99
Acacia nilotica stem (Sharma et al., 2012)	800 °C, 3 h	5.7	5.7	17.8	4.5	1.2	21.5	0.5	–	–	–	–	–	–	–
Musa acuminate peel (Pathak et al., 2018)	Burnt	-	70.06	9.54	1.78	-	4.56	7.55	3.23	1.79	-	-	-	-	1.03
Citrus sinensis peel (Changmai et al., 2021)	Burnt	-	8.95	5.01	1.30	-	-	-	-	27.54	-	-	-	-	37.20

Musa acuminata peduncle (Balajii and Niju, 2019)	Uncalcined	–	25.63	–	0.97	–	0.56	0.78	–	–	–	–	–	–	72.06
Snail shell (Laskar et al., 2018)	900 °C, 4 h	-	-	68.8	0.1	0.2	0.3	0.00	-	0.00	-	-	-	4.6	26.1

3.3.1.7 XPS studies

XPS analyses (**Fig. 3.9, 3.10**) were conducted to investigate the surface composition of BMCP, BMCS, BMCR, CMCP-550, CMCS-550, CMCR-550 and 3rd recycled CMCP-550 catalysts. The results obtained are represented in **Table 3.5** and **Table 3.6**, which indicated that the *M. champa* catalysts were composed of Na, O, C, K, Ca, Mg, Mn, Fe, Zn, Si, Sr and Cl. High concentrations of C and O were observed similar to that of the EDX data of this study. The K was found to be the most dominating metal, the highest being in 10.39 atomic % in BMCP and 18.09 atomic % in CMCP-550 catalyst, and exhibited better efficacy in the catalysis of biodiesel production compared to other catalysts of this study. Noticeably two peaks in the XPS patterns of C 1s (**Fig. 3.9** B, **Fig. 3.10** B) appeared in the burnt catalysts at binding energies of284.80 and 288.80 eV (BMCP), 284.92 and 288.72 eV (BMCS), and 284.78 and 288.70 eV (BMCR). The two peaks were observed in the calcined catalysts at binding energies of 284.92 and 288.70 eV (CMCP-550), 284.97 and 288.73 eV (CMCS-550), 284.87 and 288.50 eV (CMCR-550) and then 284.99 and 289.32 eV in the 3rd recycled CMCP-550 catalyst, which are signifying the two carbon states of C–C and C=O exhibiting the occurrence of metal carbonates in the catalysts (Tamuli et al., 2020; Eldiehy et al., 2022; Changmai et al., 2021). The XPS patterns of O 1s (**Fig. 3.9** C, **Fig. 3.10** C) showed signal at binding energy of 531.08 eV (BMCP), 531.12 eV (BMCS), 530.96 eV (BMCR), 530.57 eV (CMCP-550), 530.70 eV (CMCS-550), 530.50 eV (CMCR-550) and 531.64 eV (3rd recycled catalyst) confirming the oxygen element that existed as metal oxides in the catalysts (Pathak et al., 2018).

In the XPS patterns shown in **Fig. 3.9** D and **Fig. 3.10** D, the peak for K $2p_{3/2}$ is observed at binding energy of 292.61 eV in BMCP, 292.80 eV in BMCS, 292.64 eV in BMCR, 292.42 eV (CMCP-550), 292.54 eV (CMCS-550), 292.45 eV (CMCR-550) and 293.07 eV (3rd recycled catalyst). Similarly, the peak was observed at slightly higher binding energy for K $2p_{1/2}$ in BMCP (295.35 eV), BMCS (295.51 eV), BMCR (295.30 eV), CMCP-550 (295.19 eV), CMCS-550 (295.33 eV), CMCR-550 (295.13 eV) and 3rd recycled catalyst (295.84 eV). These two characteristic peaks appeared in **Fig. 3.9** D and **Fig. 3.10** D at two different binding energies attributed to the spin-orbit splitting of K $2p_{3/2}$ and K $2p_{1/2}$ which are accountable for the occurrence of K as +1 state in K_2O and K_2CO_3 respectively (Tamuli et al., 2020; Changmai et al., 2021). The two peaks at different binding energies for BMCP (346.60, 350.58 eV), BMCS (346.82, 350.49 eV), BMCR (346.70, 350.08 eV), CMCP-550 (346.54, 350.13 eV), CMCS-550 (346.84, 350.38 eV), CMCR-550 (346.88, 350.29 eV) and for 3rd recycled catalyst at 347.14 and 350.81 eV could be seen in XPS spectra of Ca 2p (**Fig. 3.9** E, **Fig. 3.10** E). These are more likely due to the existence of CaO and $CaCO_3$in the catalysts (Changmai et al., 2021).

Similar XPS spectra were reported for the presence of $CaCO_3$ and CaO in the catalyst by Changmai et al. (2020a), Changmai et al. (2021), Eldiehy et al. (2022) and Zhao et al. (2018). In the XPS patterns of Si 2p (**Fig. 3.9** F, **Fig. 3.10** F), a single peak was observed at 102.23 eV for BMCP, 102.29 eV for BMCS, 102.17 eV for BMCR, 101.69 eV for CMCP-550, 102.30 eV for CMCS-550, 101.69 eV for CMCR-550 and 102.67eV for the 3rd recycled catalyst, which confirmed SiO_2 component present in the catalysts. Nath et al., 2020 and Basumatary et al., 2021c also reported SiO_2 in *Sesamum indicum* and *Heteropanax fragrans* catalysts at similar binding energies. In this study, the major constituents found in the catalysts existed as metal oxides and metal carbonates due to the presence of high concentrations of O, K and C, which were confirmed by EDX and XPS studies as well as the XRD technique.

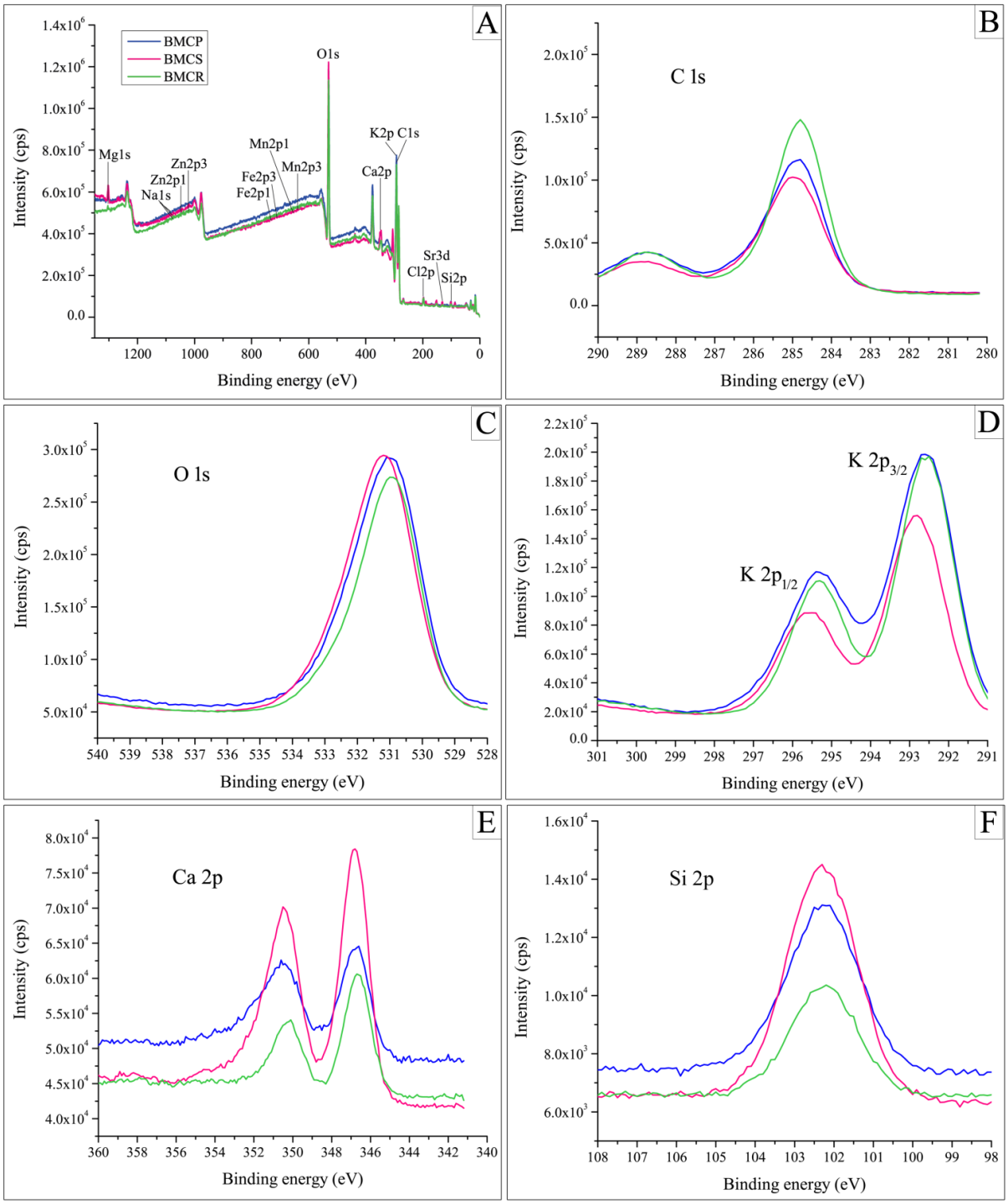

Fig. 3.9. XPS survey spectra (A) of BMCP, BMCS, BMCR catalysts; XPS patterns of C 1s (B), O 1s (C), K 2p (D), Ca 2p (E) and Si 2p (F).

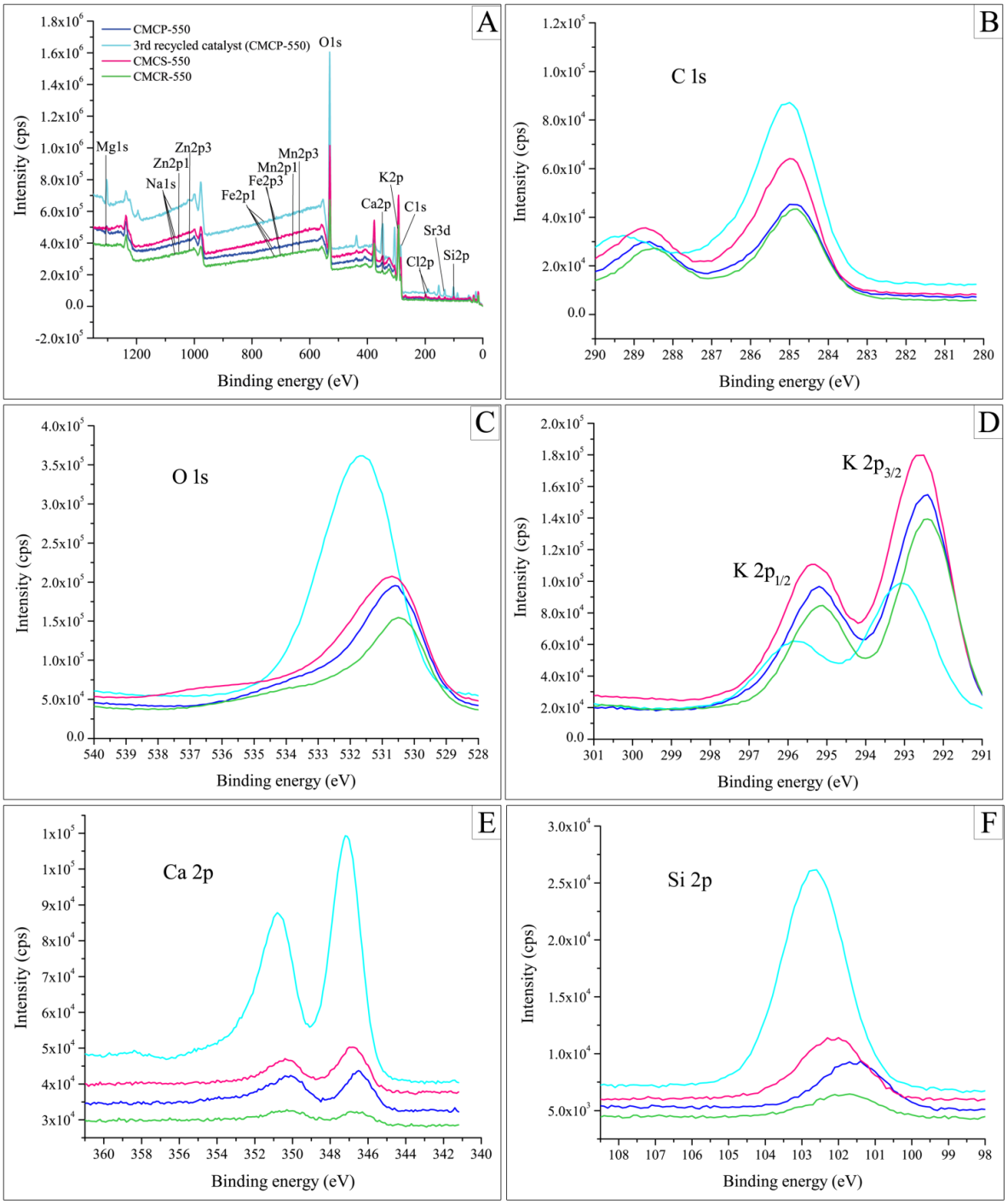

Fig. 3.10. XPS survey spectra (A) of CMCP-550, CMCS-550, CMCR-550 and 3rd recycled catalysts; XPS patterns of C 1s (B), O 1s (C), K 2p (D), Ca 2p (E) and Si 2p (F).

Table 3.5: XPS analyses of burnt *M. champa* catalysts.

Elements	Composition (Atomic %)		
	BMCP	**BMCS**	**BMCR**
Na 1s	0.09	0.16	0.07
O 1s	28.27	30.93	41.35
C 1s	54.71	42.71	47.61
K 2p	10.39	7.65	7.98
Ca 2p	1.46	2.66	0.85
Mg 1s	0.73	1.44	0.17
Mn 2p	0.20	0.34	0.35
Fe 2p	0.18	0.23	0.19
Zn 2p	0.14	0.27	0.23
Si 2p	1.90	10.83	–
Sr 3d	0.40	1.22	0.31
Cl 2p	1.54	1.58	0.85

Table 3.6: XPS analyses of calcined *M. champa* catalysts.

Elements	Composition of catalyst calcined at 550 ºC (Atomic %)			
	CMCP-550	**3rd recycled catalyst (Peel)**	**CMCS-550**	**CMCR-550**
Na 1s	0.07	–	0.09	–
O 1s	24.11	54.1	21.83	21.06
C 1s	46.03	19.31	49.91	53.53
K 2p	18.09	5.5	17.31	17.68
Ca 2p	0.23	6.3	0.22	0.18
Mg 1s	0.82	3.6	0.12	0.03
Mn 2p	0.25	0.51	0.33	0.33
Fe 2p	0.62	0.22	0.15	0.37
Zn 2p	0.30	0.26	0.16	0.18
Si 2p	8.37	7.71	8.44	5.56
Sr 3d	0.51	2.35	0.57	0.53
Cl 2p	0.62	0.14	0.85	0.56

3.3.1.8 HRTEM studies

The HRTEM images shown in **Fig. 3.11** (A-C) revealed that CMCP-550 catalyst has irregular and oval-like shapes with a porous structure. The CMCS-550 catalyst (**Fig. 3.12** A-C) showed non-uniform and irregularly shaped porous particles with a long rod-like shaped material. The catalyst CMCR-550 (**Fig. 3.13** A-C) exhibited agglomerated and porous particles with irregular sizes and shapes, and this characteristic of mesoporosity was also supported by FESEM and BET analyses. The fringes depicted in HRTEM images (**Fig. 3.11** C**, Fig. 3.12** C**, Fig. 3.13** C) are representing the characteristic of porous materials of the *M. champa* catalysts. The SAED patterns (**Fig. 3.11** D, **Fig. 3.12** D, **Fig. 3.13** D) interpreted the existence of polycrystalline materials of CMCP-550, CMCS-550 and CMCR-550 catalysts. The interplanar distances were calculated from the HRTEM images (**Fig. 3.11** C**, Fig. 3.12** C**, Fig. 3.13** C) by using the Gatan Microscopy Suite software to know the existence of polycrystalline materials of the catalysts. It is to be noted that different d-spacing values were found at different selected areas of the images that signified the polycrystalline nature of the *M. champa* base catalysts. These polycrystalline materials of the catalysts may be due to the presence of different inorganic crystalline compounds, which were also characterized by XRD studies (**Fig. 3.3**). *Sesamum indicum* and *Heteropanax fragrans* derived heterogeneous base catalysts also possessed polycrystalline nature of the materials (Nath et al., 2020; Basumatary et al., 2021c).

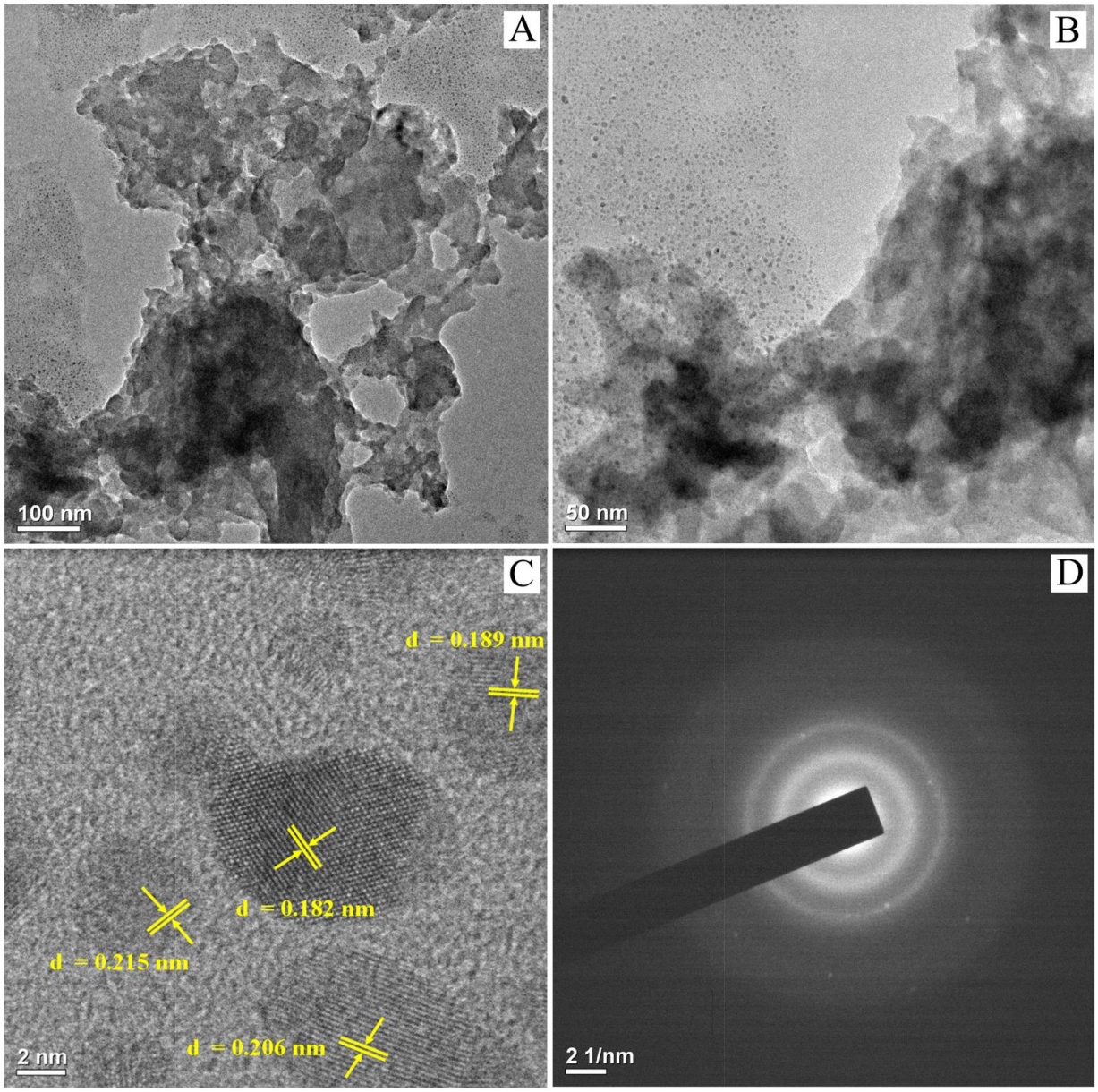

Fig. 3.11. TEM images (A–C) and SAED pattern (D) of CMCP-550 catalyst.

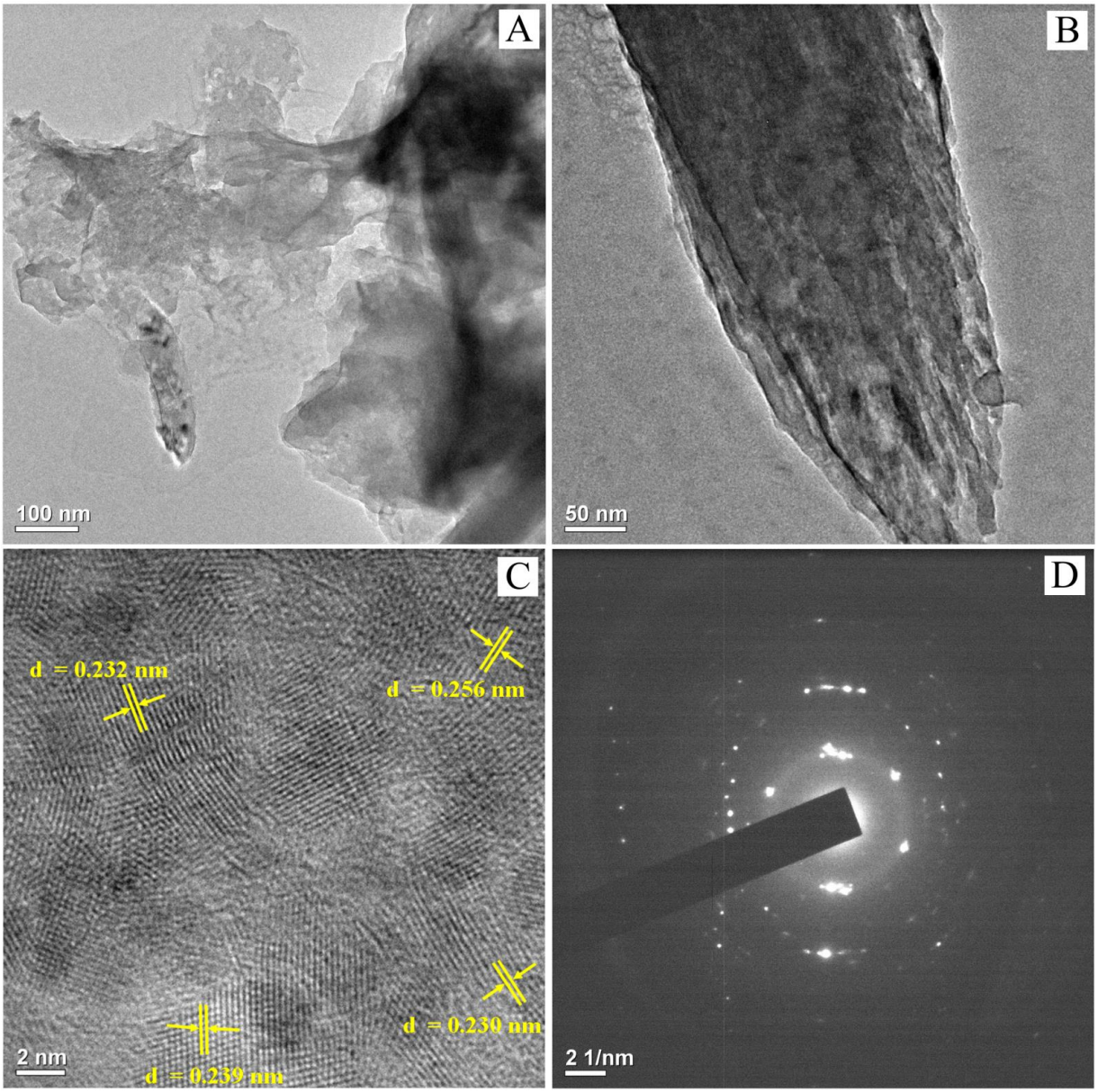

Fig. 3.12. TEM images (A–C) and SAED pattern (D) of CMCS-550 catalyst.

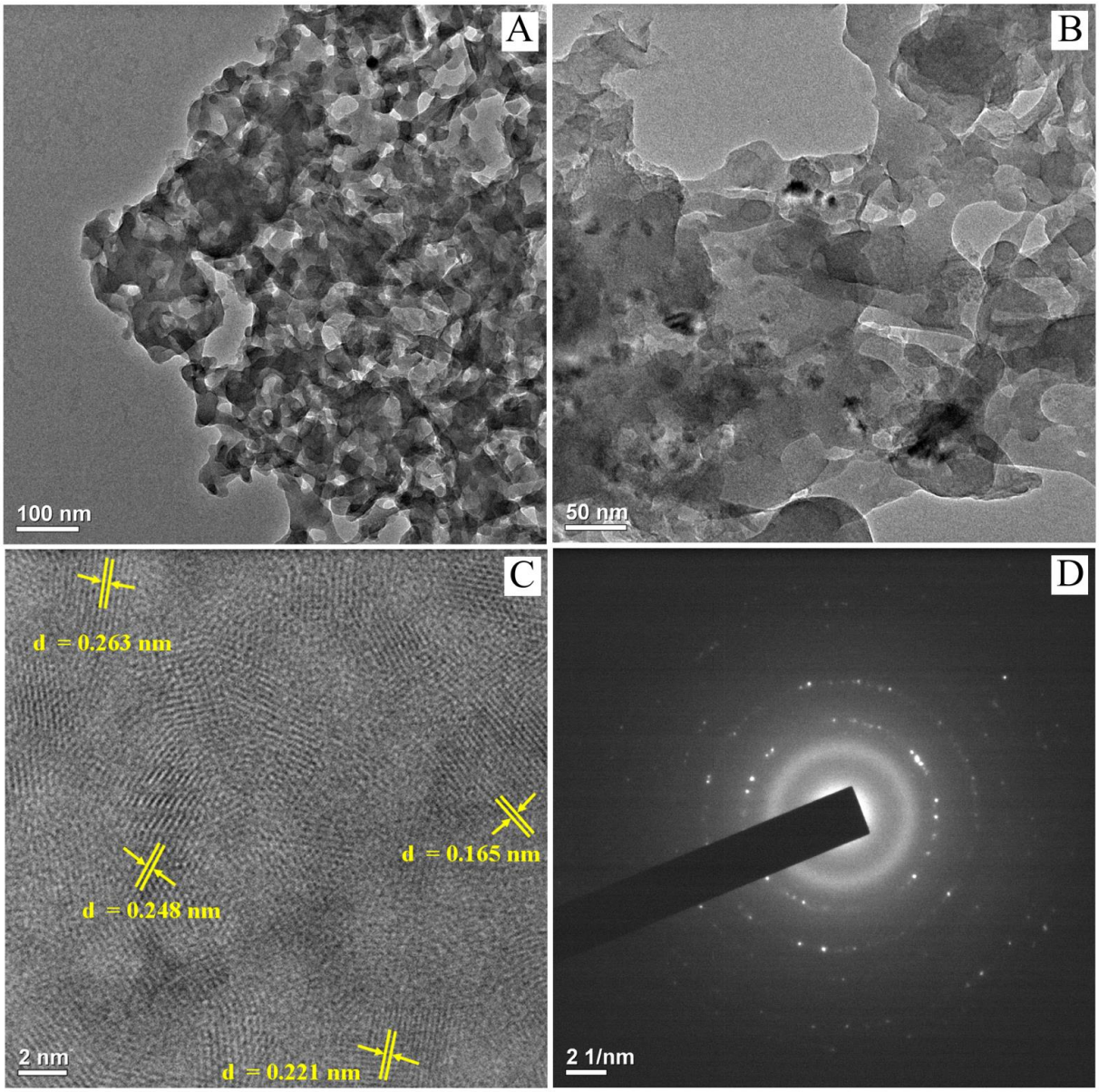

Fig. 3.13. TEM images (A–C) and SAED pattern (D) of CMCR-550 catalyst.

3.3.1.9 Determination of pH values

The pH values of CMCP-550, CMCS-550 and CMCR-550 catalysts dissolved in distilled water at 1:5, 1:10, 1:15, 1:20, 1:30 and 1:40 w/v are represented in **Fig. 3.14**. The highest pH value at 1:5 w/v was found in CMCP-550 catalyst (12.7) followed by CMCR-550 (12.4) and CMCS-550 catalyst (11.9). This trend is in strong agreement with the K contents of the catalysts exhibited by EDX (**Table 3.3**) and XPS (**Table 3.6**) studies. In this work, it was observed that the CMCP-550 catalyst having the highest pH value was highly basic that exhibited superior catalytic efficacy in biodiesel synthesis and the performance of the catalysts followed a similar trend of pH value and K content of the catalysts. Along with K, other metals

like Ca, Mg, Mn, Sr, etc. were also present in the catalysts that may contribute to the basic character of the catalysts.

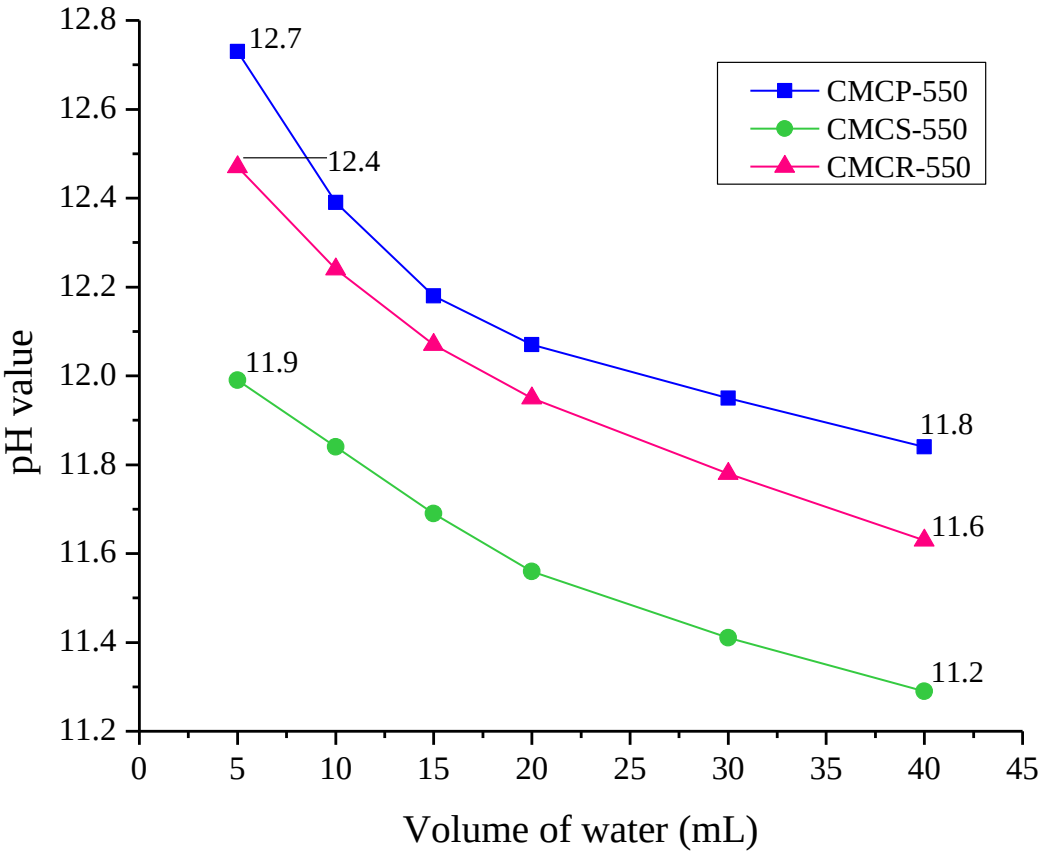

Fig. 3.14. Variation of pH values of calcined *M. champa* catalysts (1 g) with different volume of water.

3.3.1.10 Soluble alkalinity of the catalysts

The estimated soluble alkalinity values of CMCP-550, CMCS-550 and CMCR-550 catalysts were found to be 7.13, 4.77 and 5.21 mmol g^{-1} respectively. The CMCP-550 catalyst has a higher soluble alkalinity value than stem and rhizome catalysts. High soluble alkalinity may be due to the high concentrations of K, C and O present as carbonate of K and other metals in the CMCP-550 catalyst, which also displayed the highest pH value (**Fig. 3.14**). The presence of metal oxides and carbonates in the present catalysts and a higher amount of K in the CMCP-550 catalyst were supported by the characterization with XRD, FESEM-EDX and XPS techniques. Sharma et al. (2012) reported that chemically activated wood ash (calcined at 800 ^{o}C) loaded with K_2CO_3 and $CaCO_3$ gave 12.7 and 8.8 mmol g^{-1} of soluble alkalinity,

respectively which are higher compared to CMCP-550 catalyst. Mendonça et al. (2019b) also tested and described a soluble alkalinity of 3.7 mmol g^{-1} for tucumã peel catalyst.

3.3.1.11 Basicity measurement

In this study, the basic strengths of CMCP-550, CMCS-550 and CMCR-550 catalysts were found between the range of 10.1 and 18.4 (10.1<H_<18.4). From the estimation, the basicity of CMCP-550, CMCS-550 and CMCR-550 catalysts were found to be 1.25 mmol g^{-1}, 0.42 mmol g^{-1}, and 0.91 mmol g^{-1} respectively. The higher basicity of CMCP-550 catalyst is in accordance with the pH data (**Fig. 3.14**) that might be because of its highest K content depicted by EDX and XPS techniques. Other quantified basicity described by Basumatary et al. (2021c) for *Heteropanax fragrans* catalysts *viz.* CC-550 and CC-850 have the basicity value of 0.423 and 0.303 mmol g^{-1} respectively. Singh at el. (2019) also reported the basicity of 0.22 mmol g^{-1} for barium–ZnO catalyst and 0.63 mmol g^{-1} for barium-impregnated CaO-ZnO, which are slightly lower than the basicity of the catalysts of this work. In the case of catalytic activity comparison, the present catalyst CMCP-550 with higher basicity strength showed better activity in catalysis than *Heteropanax fragrans* (CC-550 and CC-850) catalysts (Basumatary et al., 2021c) and the barium-calcium-zinc mixed oxide catalyst (Singh at el., (2019).

From the obtained basicity data, the catalytic efficiencies of the present *M. champa* peel, stem and rhizome heterogeneous catalysts were determined in terms of turnover frequency (TOF) with the following mathematical equation (**3.1**). TOF describes the number of biodiesel molecules generated per unit basic active site and per unit time (Roy et al., 2020c). The TOF values in this study were found to be 14.15 h^{-1}, 6.99 $h^{-1}$and 13.84 h^{-1} for CMCP-550, CMCS-550 and CMCR-550 catalysts, respectively. The TOF value of CMCP-550 catalyst is higher in comparison to stem and rhizome catalysts as well as the TOF value reported by Roy et al. (2020c) (TOF = 4.29 h^{-1}).

$$\text{TOF} = \frac{\text{Biodiesel produced (mol)}}{\text{Basicity} \times 0.001\ (\text{mol}) \times \text{time}} \qquad (\mathbf{3.1})$$

3.3.2 Role of *M. champa* catalysts in *J. curcas* oil to biodiesel synthesis

3.3.2.1 Effect of catalyst concentration

One of the significant parameters involved in optimizing the process of biodiesel production is the effect of catalyst loading. In the present study, the effectiveness of the catalyst load of CMCP-550 catalyst was examined in the transesterification reaction. To achieve the

optimum biodiesel yield, the amount of CMCP-550 catalyst loaded was 3, 5, 7 and 9 wt. % of oil and the reaction performed was at a constant reaction temperature of 65 ^{o}C and the MTOMR used was 9:1 (**Fig. 3.15**). It was observed that the reaction time decreased with an increase in the concentration of catalyst amount (wt. %). On the other hand, the yield % of biodiesel increased with the amount of catalyst loading from 3 to 5 wt. %, which may be due to an increase in the number of active sites in the catalyst (Laskar et al., 2018; Roschat et al., 2016). However, on loading the catalyst more than 5 wt. %, the yield % gradually decreased as shown in **Fig. 3.15**. The reason for decreasing yield % when loaded beyond 5 wt. % may be due to poor diffusion of the reaction mixture. Excess loading of the catalyst turns the mixture phase more viscous which leads the difficulty in the conversion of oil into FAME which is caused by the limitation of mass transfer among the reactants (Gohai et al., 2020; Laskar et al., 2018; Roschat et al., 2016). Moreover, the employment of excess catalyst concentration may result in soap formation leading to a decrease in biodiesel yield (Dhawane et al., 2016). In this study, the catalyst CMCP-550 with 5 wt. % showed noteworthy results (**Fig. 3.15**) at 65 ^{o}C and 9:1 MTOMR in 10 min. Thus, 5 wt. % is considered the optimum catalyst amount for this study.

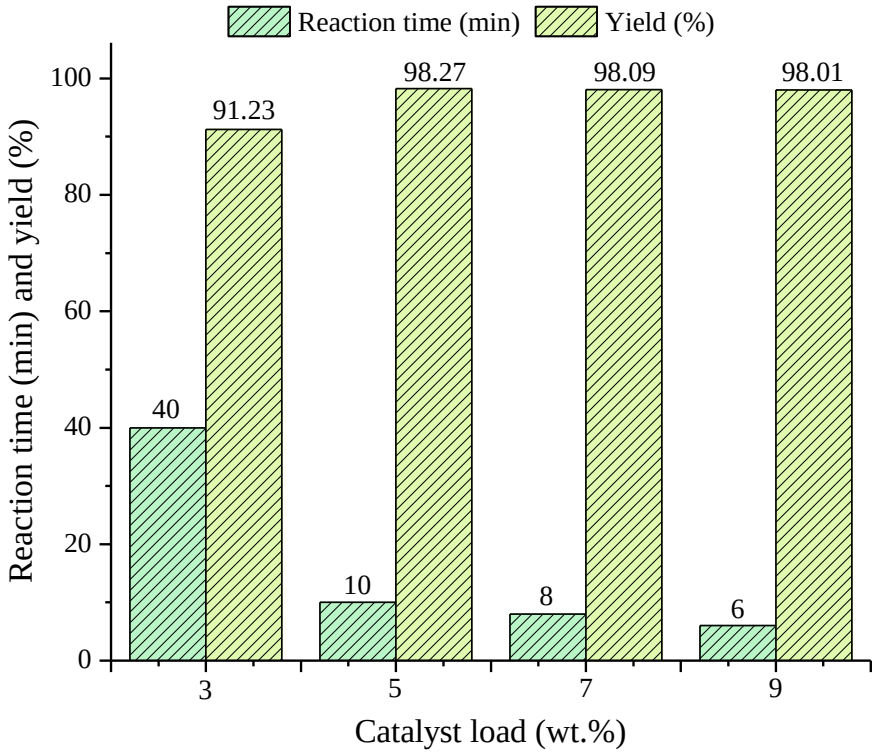

Fig. 3.15. Effect of catalyst loading of calcined *M. champa* peel (CMCP-550) on biodiesel synthesis (Temperature = 65 ^{o}C, MTOMR = 9:1).

3.3.2.2 Effect of MTOMR

MTOMR is an essential factor that greatly influences the transesterification reaction. In the present study, various reactions loaded with 5 wt. % of CMCP-550 catalyst at 65 ^{o}C were carried out to examine the effect of MTOMR of 3:1, 6:1, 9:1, 12:1, 15:1 and 18:1. It was observed that on increasing the MTOMR from 3:1 to 9:1, both the yield % of biodiesel and reaction time improved significantly (**Fig. 3.16**). At 9:1 MTOMR, the yield reached to the maximum of 98.27 % in the reaction time of 10 min. On the further increase of MTOMR greater than 9:1the yield %of biodiesel as well as the reaction time drops downs lightly (**Fig. 3.16**). This is because of the reason that the catalyst is deactivated with the larger amount of methanol. Moreover, excessive methanol lowers the relative concentration of oil and may also shift the reaction from equilibrium into reverse. The byproduct glycerol formed also dissolves in the excess methanol and causes the separation difficult from biodiesel (Singh et al., 2019, Shan et al., 2015). From a stoichiometric perspective, the transesterification reaction requires 3 moles of methanol and 1 mole of oil to obtain the product of 3 moles of biodiesel and 1 mole of glycerol (Singh et al., 2019; John et al., 2020). However, utilization of a higher amount of methanol up to a certain optimum level is essential to drive the equilibrium towards the direction of enhancing the yield % of methyl esters. The excess amount of methanol also promotes the reaction rate and removes product molecules from the surface of the catalyst and thereby regenerating the active catalyst sites (Kataria et al., 2018). Accordingly, in the present study, MTOMR 9:1 is considered the optimal ratio for the synthesis of biodiesel.

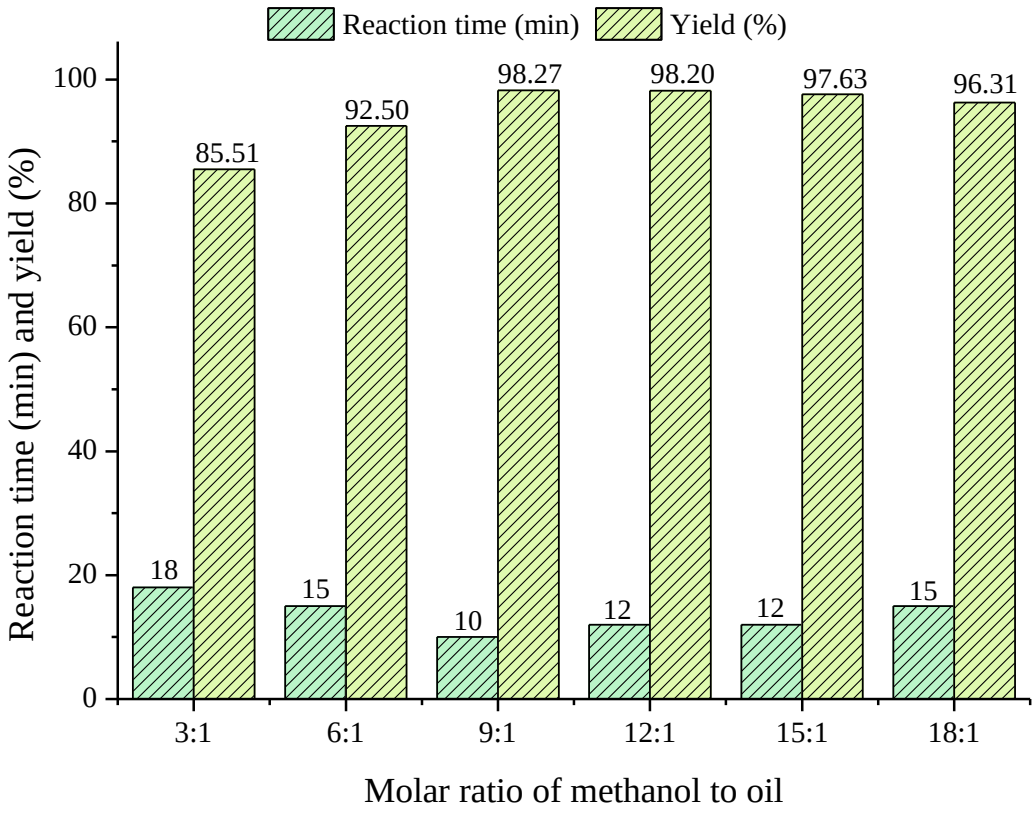

Fig. 3.16. Effect of MTOMR on biodiesel synthesis (Temperature = 65 ^{o}C, CMCP-550 catalyst = 5 wt.%).

3.3.2.3 Effect of temperature on the reaction

The effect of temperature was examined by setting transesterification reactions at various temperatures (35 ^{o}C, 45 ^{o}C, 55 ^{o}C, 65 ^{o}C and 75 ^{o}C) using CMCP-550 catalyst for the production of biodiesel at the optimum 9:1 MTOMR and 5 wt. % of catalyst. In this study, the two other calcined catalysts *viz.* CMCS-550 and CMCR-550 were also tested under the same reaction conditions to know the efficacies of different catalysts and the results are represented in **Fig. 3.17** (A, B). It was observed that increase in temperature from 35 to 65 ^{o}C, the activities of the catalysts increased sharply showing a rapid decline in the reaction time (**Fig. 3.17** A), however, no significant change in the reaction time was observed when the temperature is raised from 65 ^{o}C to 75 ^{o}C. It was also noticed that the biodiesel yield achieved at 65 ^{o}C was the maximum (**Fig. 3.17** B) with all three catalysts employed. Beyond 65 ^{o}C i.e., at 75 ^{o}C, the yield of biodiesel slightly decreased which may be because the methanol vaporizes, creating bubbles and hindering the reaction system (Liu et al., 2008a; Meng et al., 2008). It is seen that better results were displayed at 65 ^{o}C (**Fig. 3.17** A, B) and it can be considered the optimum

temperature. Thus, the optimum reaction conditions (ORCs) of this study were 9:1 MTOMR and 5 wt. % of catalyst at 65 ^{o}C.

At the ORCs of this study, the CMCP-550 catalyst demonstrated the best catalytic activity in biodiesel synthesis that yielded 98.27 % of the product in 10 min and the order of catalytic activity is CMCP-550 > CMCR-550 (97.89 % in 14 min) > CMCS-550 (97.78 % in 60 min). This reactivity in catalysis was because of the basic strengths of the catalysts and the basicity was also in the similar order of CMCP-550 (1.25 mmol g^{-1}) > CMCR-550 (0.91 mmol g^{-1}) > CMCS-550 (0.42 mmol g^{-1}). This trend is in strong agreement with the pH values (**Fig. 3.14**) and the K concentrations of the catalysts depicted by EDX (**Table 3.3**) and XPS (**Table 3.6**) studies. The *M. champa* burnt ash catalysts i.e., BMCP, BMCS and BMCR catalysts were also examined in biodiesel synthesis from *J. curcas* oil at the same ORCs, and the results are depicted in **Fig. 3.18.** The catalytic activities of these catalysts are found in the order of BMCP > BMCR > BMCS, the best one being the BMCP catalyst that could produce a high biodiesel yield 96.70 % in 45 min. This trend is also in good agreement with the K contents of the burnt ash catalysts (**Table 3.2**, **Table 3.5**). Thus, it can be concluded that the calcined peel catalyst (CMCP-550) is showing the best and superior efficacy among the different calcined and burnt ash catalysts of this study and this is because of its stronger basicity, which was accredited due to its higher K concentration occurring as K_2CO_3 and K_2O (**Fig. 3.3**). Further, the catalyst becomes more active when it is activated by calcination at certain temperatures due to generation of more active sites.

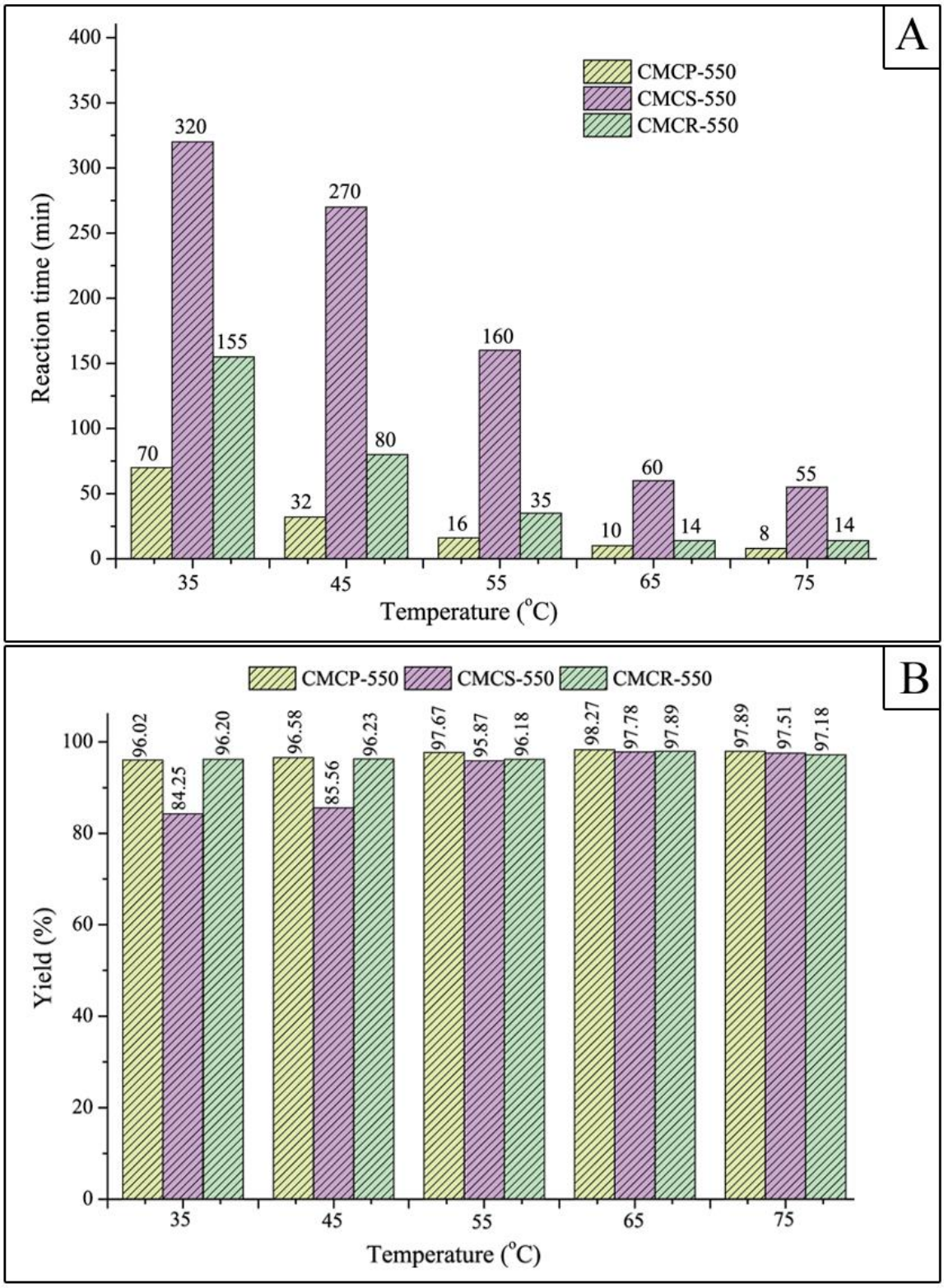

Fig. 3.17. Effect of temperatures on biodiesel synthesis. Reaction conditions (MTOMR = 9:1, CMCP-550, CMCS-550 and CMCR-550 catalysts = 5 wt.%).

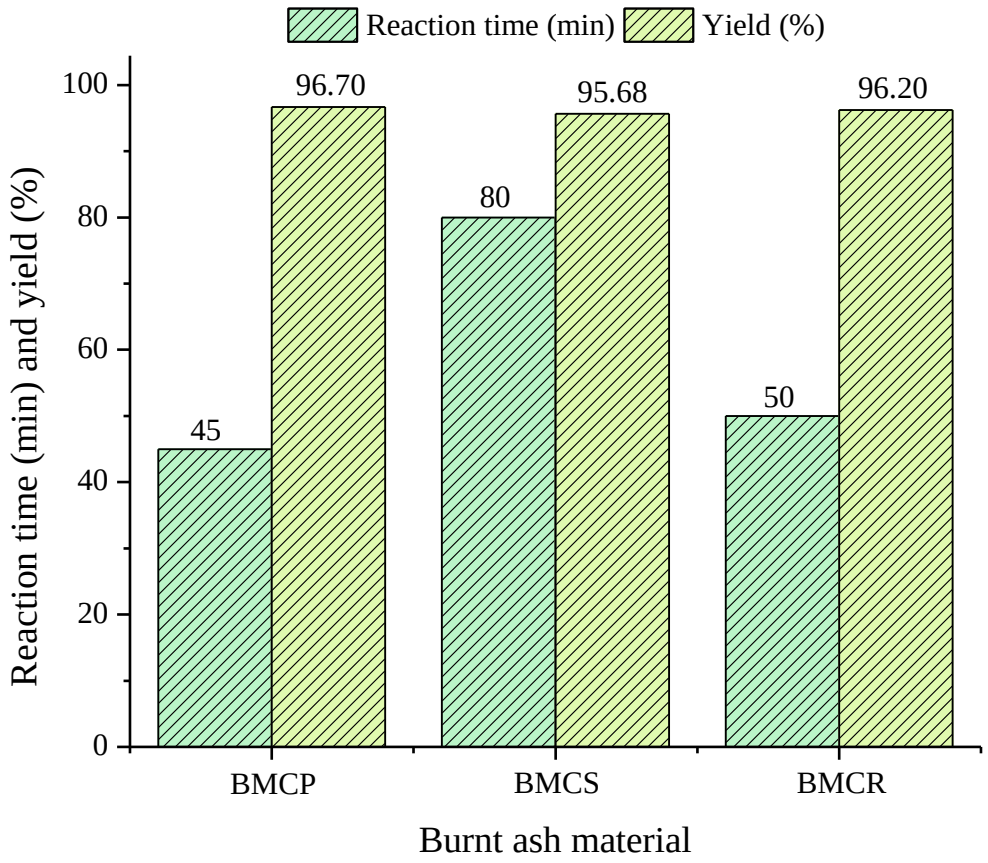

Fig. 3.18. Catalytic activities of the BMCP, BMCS and BMCR catalysts in biodiesel production. Reaction conditions (Temperature = 65 ^{o}C, MTOMR = 9:1, catalysts = 5 wt.%).

3.3.2.4 Reusability studies of *M. champa* catalyst

The recyclability of catalysts is an advantageous factor because it can reduce the production cost, and material needed. In this study, the reusability test of the best catalyst (CMCP-550) was conducted at ORCs. The utilized CMCP-550 catalyst was regenerated from the first reaction by filtration through Whatman no. 42 using a suction pump. The catalyst recovered was rinsed four times with petroleum ether and then washed out with acetone to remove any remaining products, glycerol and other impurities. The washed catalyst was spread over a petri-dish and allowed to dry in a hot air oven at 110 ^{o}C for 4 h. After that, the dried catalyst was cooled in a desiccator and used in the subsequent reaction, and a similar protocol was maintained for each reaction cycle. The results of reusability studies are represented in **Fig. 3.19**, which displayed a gradual decrease in catalytic activities at every cycle of the reaction. The yield of biodiesel decreased from 98.27 % (fresh reaction) to 93.79% (3rd cycle) with a significant increase in reaction time. The 3rd recycled catalyst was characterized using FT-IR (**Fig. 3.4**), FESEM-EDX (**Fig. 3.8**) and XPS (**Fig. 3.10**) techniques to know any changes

in the catalyst after the reuse. The morphological changes were observed by comparing the FESEM image of the fresh CMCP-550 catalyst (**Fig. 3.7** A) with the FESEM images of the 3rd recycled (CMCP-550) catalyst (**Fig. 3.8** A-C). The fresh catalyst was more packed and agglomerated with clusters of oval-like and spongy shapes, whereas the 3rd recycled catalyst changed into needle-like strips shape as if washed away with some solvent and possibly coated with glycerol or esters. It is evident from the EDX data (**Table 3.3**) that the K content of CMCP-550 catalyst was reduced from 47.49 wt. % to 11.37 % in the 3rd recycled catalyst, which played a major role in the catalysis of this study. XPS study also showed that 18.09 atomic % of K in CMCP-550 catalyst was reduced to 5.5 atomic % in the recycled catalyst (**Table 3.6**) indicating the leaching of active components that may also cause the loss of active sites of the catalyst. This decrease in the concentration of K due to its leaching during the recycling of the catalyst is one of the main reasons for the reduced catalytic activity in biodiesel synthesis of this work. In the 3rd recycled catalyst shown in **Fig. 3.4**, the appearance of the declined peak intensity of carbonates (CO_3^{2-}) at 1641, 1469 cm^{-1} and 1419 cm^{-1} may ascribe to the slight decrease in K_2CO_3 concentration. In addition, a weak peak at 2928 cm^{-1} in the FT-IR spectrum (**Fig. 3.4**) was observed demonstrating the C-H bond vibration which is most likely due to the agglomeration of glycerol molecule on the surface of the catalyst that leads to the blockage of the active sites and resulted in a decrease in the catalytic activity of the recycled catalyst.

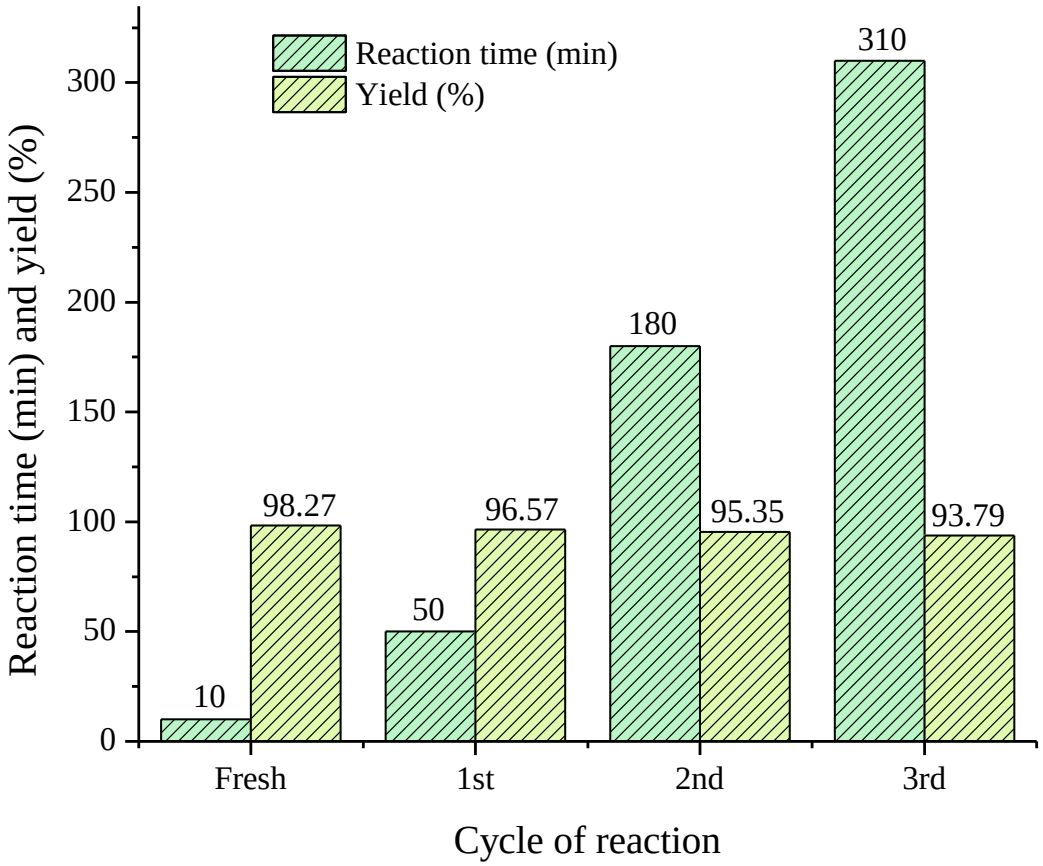

Fig. 3.19. Reusability of calcined *M. champa* peel (CMCP-550) catalyst (Reaction temperature = 65 ^{o}C, MTOMR = 9:1, catalyst loading = 5 wt.%).

3.3.2.5 Activation energy of the reaction

The activation energies of the reactions of *J. curcas* oil and methanol using CMCP-550, CMCS-550 and CMCR-550 catalysts at different temperatures (35, 45, 55, 65 and 75 ^{o}C) were evaluated from the Arrhenius equation of pseudo-first-order reaction (Nath et al., 2019; Kaur and Ali, 2015). In this study, rate constants (k) were first calculated and found to be 0.05, 0.11, 0.23, 0.41 and 0.48 min^{-1}using CMCP-550 catalyst, 0.01, 0.01, 0.02, 0.06 and 0.07 min^{-1} using CMCS-550 catalyst and 0.02, 0.04, 0.09, 0.28 and 0.25 min^{-1} using CMCR-550 catalyst. Finally, the calculated activation energies of the reactions catalyzed by the CMCP-550 catalyst (54.256 kJ mol^{-1}), CMCS-550 catalyst (63.150 kJ mol^{-1}) and CMCR-550 catalyst (61.677 kJ mol^{-1}) are found to be within 21–84 kJ mol^{-1} reported for biodiesel synthesis reaction (Nath et al., 2019; Kaur and Ali, 2015). Among the three calcined catalysts, the reaction with the CMCP-550 catalyst showed the lowest activation energy, converting the oil feedstock into biodiesel in less reaction time and it was a chemically controlled reaction. In this study, the frequency factors were also calculated by substituting the values of slope and intercept obtained

from the Arrhenius plot (**Fig. 3.20)** and found to be 8.44 × 10^7 min^{-1}, 2.43 × 10^8 min^{-1} and 6.19 × 10^8 min^{-1} for CMCP-550, CMCS-550 and CMCR-550 catalysts, respectively.

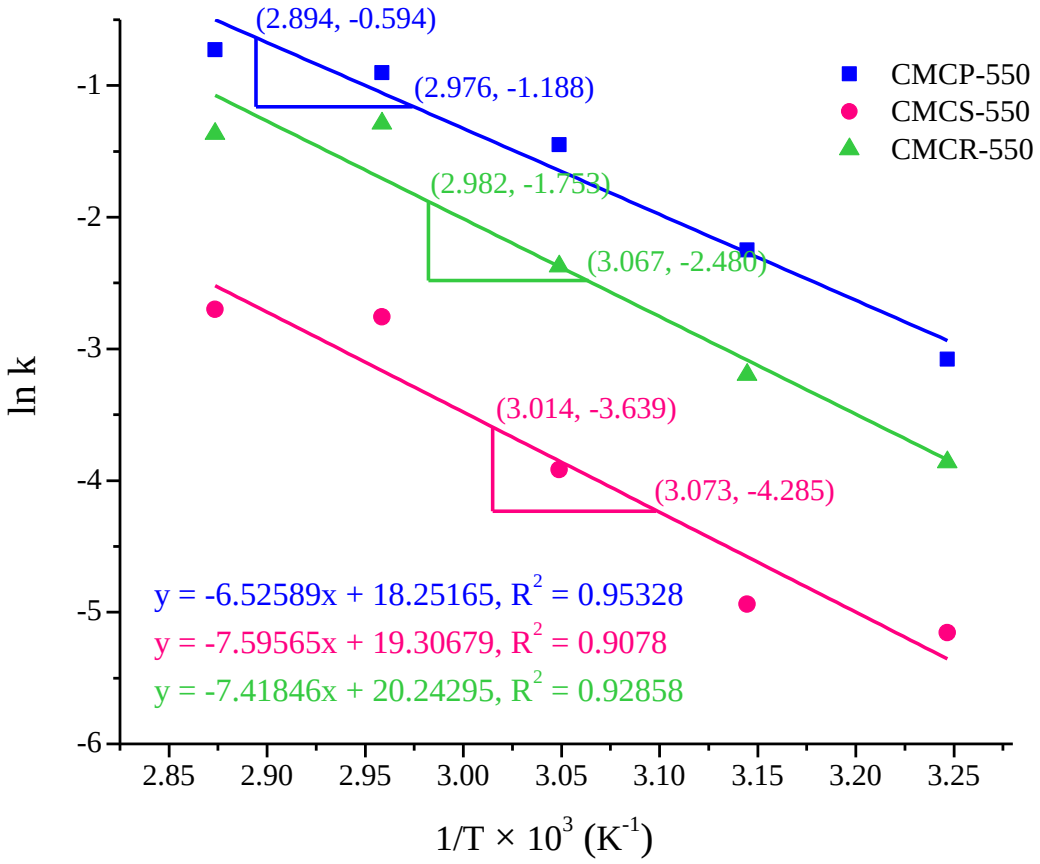

Fig. 3.20. Arrhenius plot (ln k versus 1/T×10^3) employing *M. champa* catalysts (Reaction temperatures = 35, 45, 55, 65 and 75 ^oC).

3.3.3 Comparison of *M. champa* catalysts with reported catalysts derived from waste biomasses

Among the different burnt and calcined *M. champa* catalysts of the present work, the calcined *M. champa* peel (CMCP-550) catalyst having a higher concentration of K (47.49 %) (**Table 3.3, Table 3.6**) and slightly more surface area of 6.848 m^2 g^{-1} demonstrated the best catalytic activity. This catalyst could yield 98.27 % of biodiesel from *J. curcas* oil in 10 min under the ORCs of 9:1 MTOMR and 5 wt. % catalyst at 65 ^oC. The superior catalytic activity of this catalyst was due to its higher basic character (basicity of 1.25 mmol g^{-1}, **Fig. 3.14**). In this study, the TOF of the catalysts was found in the order of 14.15 h^{-1} (CMCP-550) > 13.84 h^{-1} (CMCR-550) > 6.99 h^{-1} (CMCS-550). In this study, the comparisons of *M. champa* catalysts in biodiesel synthesis with other reported waste biomass-based solid catalysts are listed in

Table 3.7. The high conversion of biodiesel was reported with a longer reaction time by Gohain et al. (2017) using a banana peel catalyst containing 41.37 % of K and by Balajii and Niju (2019) using *Musa acuminate* peduncle catalyst whose K composition was 42.23 %. The catalytic efficacies of these catalysts are lower than the present CMCP-550 catalyst which may be due to the containment of lower K in their catalyst. Nath et al. (2019; 2020) used *Brassica nigra* and *Sesamum indicum* catalysts in biodiesel production. Their catalysts also contained a good amount of K as carbonate and oxide and reported slightly lower efficacies with higher catalyst dosages (7 wt. %). Sarma et al. (2014) and Aslam et al. (2014) reported the use of *M. balbisiana* underground stem (MBUS) catalyst that possessed a lesser amount of K_2O (25.09 %) and K (16.83 %). They reported a catalyst surface area of 38.7 $m^2 g^{-1}$ which is higher than that of the present catalyst, but when it was applied in a transesterification reaction with a higher temperature of 275 ^oC along with longer reaction time for high conversion compared to the present CMCP-550 catalyst. This lower efficacy may be due to the lower basicity of their catalyst. The catalyst derived from pineapple leaves studied by Junior et al. (2020) revealed a higher reaction time (30 min) with the usage of the excessive amount of methanol (40:1) indicating lower catalytic activity compared to the CMCP-550 catalyst. The activation energy of their reaction was 86.84 kJ mol^{-1}, which is higher than the CMCP-550 catalyzed reaction (54.256 kJ mol^{-1}) signifying lower activity of pineapple leaves-based catalyst. The reason may be due to the lower concentration of alkali and alkaline earth metals in their catalyst. Several solid catalysts derived from waste biomass sources were evaluated in the synthesis of biodiesel by using $CaCO_3$-*Acacia nilotica* (Sharma et al., 2012), *Lemna perpusilla* (Chouhan and Sarma, 2013), *Carica papaya* peel (Etim et al., 2021) and *Moringa oleifera* leave (Aleman-Ramirez et al., 2021). The performances of these catalysts were poor with a lower yield of biodiesel (**Table 3.7**). Additionally, Pathak et al. (2018), Betiku et al. (2016) and Odude et al. (2019) utilized banana peel catalysts from different species and Olatundun et al. (2020) studied cocoa pod husk-plantain peel and they reported higher biodiesel yield but the reaction completion time for conversion was higher than the present catalyst indicating that present catalysts are more active. The present CMCP-550 and CMCR-550 catalysts showed better catalytic activities than the catalyst derived from *Heteropanax fragrans* (Basumatary et al., 2021c), and pawpaw peel (Oladipo et al., 2020) that contained lower K elements. The catalysts like tucumã peel (Mendonca et al., 2019b) and SrO-MBUS (Kumar et al., 2016) also exhibited higher reaction time and temperature indicating lower activities than the present *M. champa* catalysts. Several studies of solid catalysts derived from waste biomass sources have also been reported in the synthesis of biodiesel by Deka and Basumatary (2011), Gohain et al. (2020a), Arumugam and

Sankaranarayanan (2020). They reported lower catalytic activities signifying that the present catalyst was the most capable of synthesizing biodiesel. Changmai et al. (2021), Laskar et al. (2018) and Niju et al. (2021) also stated longer reaction times and lower catalytic activities compared to the catalysts of this study. A notable common characteristic of the reported catalysts was that most of these catalysts contained lower K concentration which might be the reason for displaying the low efficacies in the reaction. Thus, it is evident that the catalyst with a higher composition of K as oxide and carbonate promotes the transesterification reaction for faster production of biodiesel. That is why the present CMCP-550 catalyst possessing 47.49 % of K in it is the most capable of synthesizing the biodiesel within a very short reaction time with a highly satisfactory yield.

Table 3.7: Comparison of *M. champa* catalysts in biodiesel synthesis with other reported waste biomass based solid catalysts.

Biodiesel feedstock	**Catalyst**	**Surface area ($m^2 g^{-1}$)**	**Parameters**				**Biodiesel, Y or C (%)**	**References**
			MTOMR	**Catalyst (wt. %)**	**Temp (°C)**	**Time (min)**		
J. curcas oil	CMCP-550 (peel)	6.848	9:1	5	65	10	98.27 (Y)	This work
J. curcas oil	CMCS-550 (Stem)	1.388	9:1	5	65	60	97.78 (Y)	This work
J. curcas oil	CMCR-550 (rhizome)	0.876	9:1	5	65	14	97.89 (Y)	This work
WCO	MB peel	14.0	6:1	2	60	180	100 (C)	(Gohain et al., 2017)
Ceiba pentandra oil	MA peduncle	45.9	11.46:1	2.68	65	106	98.73 (C)	(Balajii and Niju, 2020)
Soybean oil	*Brassica nigra*	7.3	12:1	7	65	25	98.79 (Y)	(Nath et al., 2019)
Sunflower oil	*Sesamum indicum*	3.6	12:1	7	65	40	98.9 (Y)	(Nath et al., 2020)
J. curcas oil	MBUS	38.7	9:1	5	275	60	98 (Y)	(Sarma et al., 2014)
Mesua ferrea oil	MBUS	38.7	9:1	5	275	60	95 (C)	(Aslam et al., 2014)
Soybean oil	Pine apple leaves	–	40:1	4	60	30	98 (Y)	(Junior et al., 2020)
J. curcas oil	$CaCO_3$-*Acacia nilotica* ash	14.0	12:1	5	65	180	91.7 (C)	(Sharma et al., 2012)
J. curcas oil	*Lemna perpusilla*	9.6	9:1	5	65	300	89.43 (Y)	(Chouhan and Sarma, 2013)

Used vegetable oil	*Carica papaya* peel	–	12:1	3.5	65	60	97.5 (Y)	(Etim et al., 2021)
Soybean oil	*Moringa oleifera* leaves	–	6:1	6	65	120	86.7 (Y)	(Aleman-Ramirez et al., 2021)
Bauhinia monandra oil	Banana peel	4.4	7.6:1	2.75	65	69	98.5 (C)	(Betiku et al., 2016)
Soybean oil	MA peel	1.4	6:1	0.7	RT	240	98.95 (C)	(Pathak et al., 2018)
Palm oil	Banana peel	4.4	3:2.4	4	65	65	99 (Y)	(Odude et al., 2019)
Honne oil	Cocoa pod husk-plantain peel	18.86	15:1	4.5	65	150	98.98 (Y)	(Olatundun et al., 2020)
J. curcas oil	*Heteropanax fragrans*	27.50	12:1	7	65	65	97.75 (Y)	(Basumatary et al., 2021c)
Moringa oleifera oil	Pawpaw peel	3.6	9:1	3.5	35	40	96.43 (Y)	(Oladipo et al., 2020)
Soybean oil	Tucumã peel	1.0	15:1	1	80	240	97.3 (C)	(Mendonça et al., 2019b)
J. curcas oil	SrO-MBUS	0.04	9:1	5	200	60	96 (Y)	(Kumar et al., 2016)

Thevetia peruviana oil	MB stem	1.4	20:1	20	32	180	96 (Y)	(Deka and Basumatary, 2011)
WCO	*Carica papaya* stem	78.6	9:1	2	60	180	95.23 (C)	(Gohain et al., 2020a)
Calophyllum inophyllum oil	Residual ash from sugarcane leaves	–	19:1	5	64	180	97 (Y)	(Arumugam and Sankaranarayanan, 2020)
Soybean oil	Snail shell	7.0	6:1	3	28	420	98 (Y)	(Laskar et al., 2018)
WCO	*Citrus sinensis* peel ash@Fe_3O_4	15.55	6:1	6	65	180	98 (Y)	(Changmai et al., 2021)
Madhuca indica oil	Poovan banana pseudostem	4.58	14.9:1	5.9	65	178	97.97 (C)	(Niju et al., 2021)

WCO–Waste cooking oil; Temp–temperature; RT–room temperature; C–conversion; Y–yield; MTOMR–molar ratio of methanol to oil; wt–weight; min–minute; MBUS–*Musa balbisiana* underground stem; MA–*Musa acuminata*; MB–*Musa balbisiana.*

3.3.4 FTIR, NMR and GC-MS studies of biodiesel

In this study, the most noticeable absorption peak at 1746 cm^{-1} ascribed to glyceride linkage in *J. curcas* oil is due to carbonyl C=O stretching vibration (**Fig. 3.21**). This strong peak is shifted at 1742 cm^{-1}due to C=O stretching vibration of esters of biodiesel (**Fig. 3.21**), which is representing the conversion of oil into biodiesel (Nath et al., 2019). The peak at 3007 cm^{-1} observed both in oil and biodiesel is signifying the C-H bond vibration of –CH=CH– group. The bands at 2930 cm^{-1} and 2853 cm^{-1} in the oil and the band at 2927 and 2859 cm^{-1} in the biodiesel are indicating the C-H stretching vibrations of the fatty acid chain. The peak at 1648 cm^{-1} (oil) and 1654 cm^{-1} (product) is due to C=C stretching vibration of the unsaturated chain. The peaks at 1459 and 1371 cm^{-1} for oil, and at 1466, 1439 and 1358 cm^{-1} for biodiesel are due to CH_3 bending vibrations. The presence of ester molecules and the C-O bond vibrations are exhibited by the peaks at 1231, 1163 and 1096 cm^{-1} in oil and, at 1244, 1196, 1169 and 1015 cm^{-1} in the biodiesel. The peak observed at 719 cm^{-1} in oil and 725 cm^{-1} in the produced biodiesel reveals the $–CH_2–$ rocking of fatty acid long chains (Falowo and Betiku, 2022).

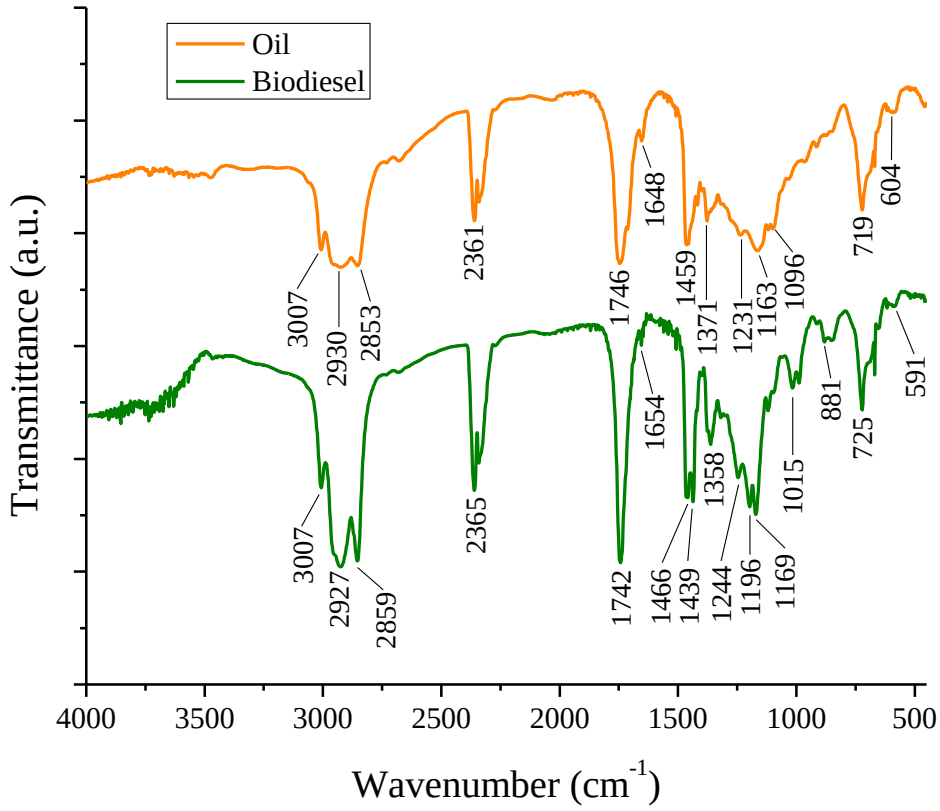

Fig. 3.21. FT-IR spectra of *J. curcas* oil and its biodiesel.

Various types of protons recorded through ^{1}H NMR spectral analyses of *J. curcas* oil (**Fig. 3.22**) and biodiesel (**Fig. 3.23**) are represented in **Table 3.8**. After transesterification of *J. curcas* oil, one new signal for the methoxy protons (OC***H***$_3$) of biodiesel is observed at δ 3.573 ppm in **Fig. 3.23** indicating the formation of biodiesel. It can also be clearly noted that the disappearance of the signals responsible for methine proton of C2 of triglycerides (-C***H***-CO_2R) at δ 5.251–5.270 ppm and for methylene protons of C1 and C3 of triglycerides (-C***H***$_2$-CO_2R) at δ 4.122–4.318 ppm was observed in **Fig. 3.23**, however, these signals were remarkably seen in **Fig. 3.22** before the transesterification reaction. These changes in the signals are indicative of product formation.

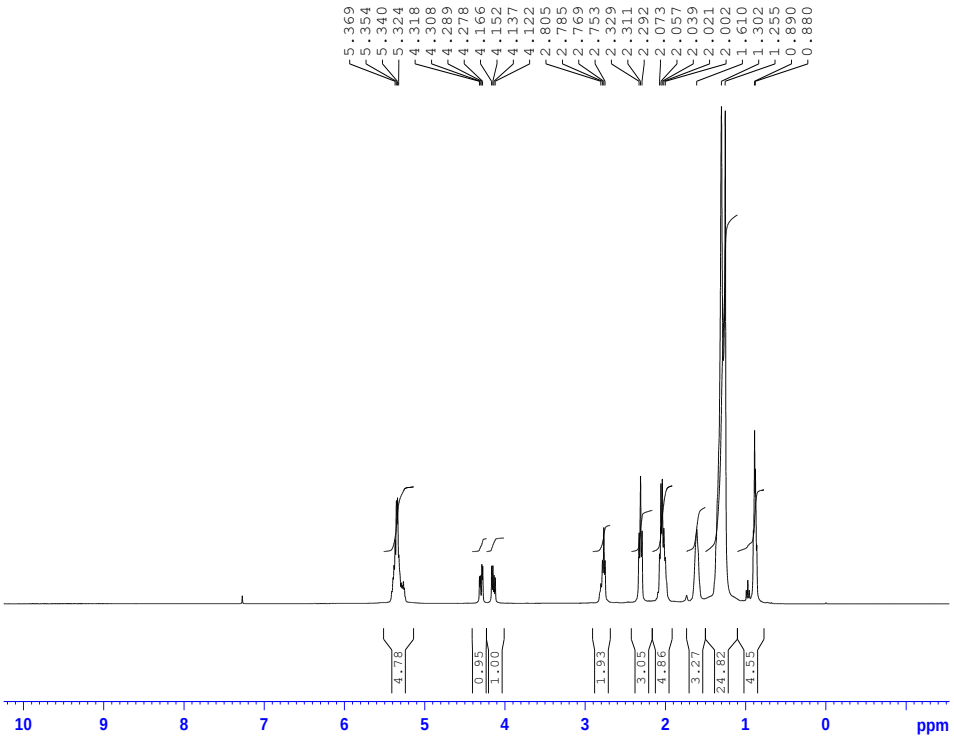

Fig. 3.22. ^{1}H NMR spectrum of *J. curcas* oil.

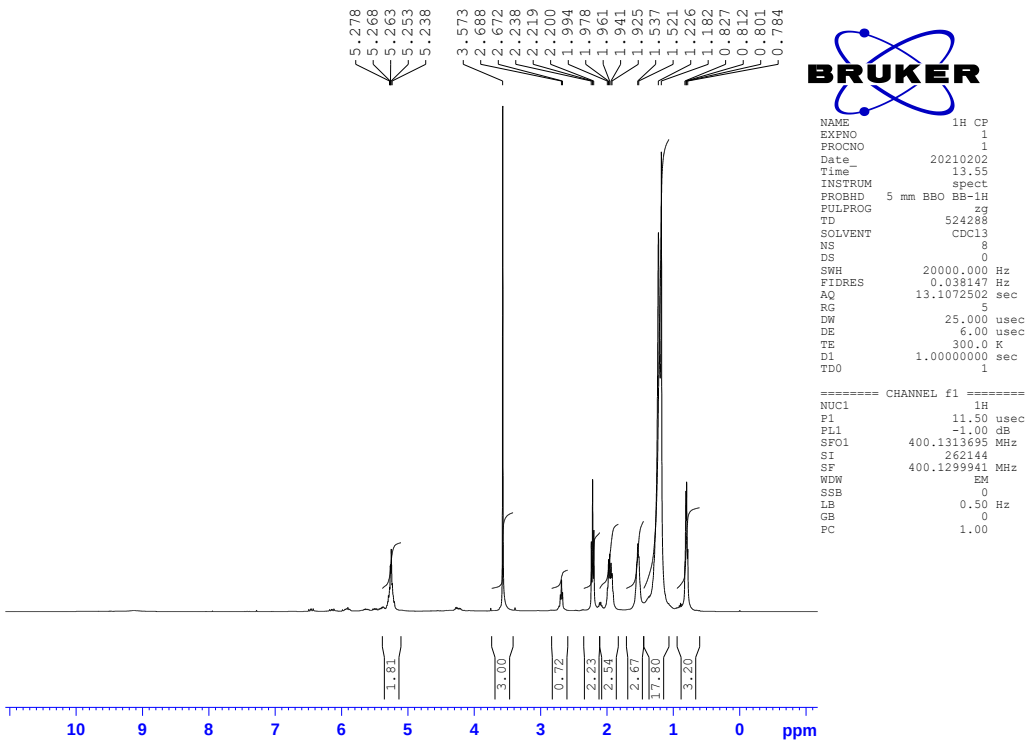

Fig. 3.23. ^{1}H NMR spectrum of jatropha biodiesel.

Table 3.8: NMR spectral analyses of *J. curcas* oil and biodiesel.

Types of protons	***J. curcas* oil**	**Biodiesel**
	^{1}H NMR (δ, ppm)	**^{1}H NMR (δ, ppm)**
Olefinic protons (-CH=CH-)	5.324–5.369	5.278–5.238
Methine proton at C2 of glycerides (-CH-CO_2R)	5.251–5.270	-
Methylene protons at C1 and C3 of glycerides (-CH_2-CO_2R)	4.122–4.318	-
Methoxy protons (-$COOCH_3$) of esters	-	3.573
Bis-allylic protons (-C=C-CH_2-C=C-)	2.753–2.805	2.672–2.688
α-methylene to ester (-CH_2-CO_2R)	2.292–2.329	2.200–2.238
α-methylene to double bond (-CH_2-C=C-)	2.002–2.073	1.925–1.994
β-methylene to ester (CH_2-C-CO_2R)	1.610	1.521–1.537
Backbone methylenes -$(CH_2)_n$-	1.255–1.302	1.182–1.226
Terminal methyl protons (C-CH_3)	0.880–0.890	0.784–0.827

The composition of jatropha biodiesel was investigated through the GC-MS technique (**Fig. 3.24**) and identified based on the library match software (TurboMass NIST 2008) is presented in **Table 3.9**. The dominant unsaturated fatty acid methyl ester contained in the biodiesel is methyl oleate (45.575 %) followed by two other unsaturated fatty acid esters viz. methyl linoleate (19.518 %) and methyl gondoate (1.106 %). Three saturated compounds such as methyl palmitate (25.205 %), methyl stearate (6.051 %) and methyl arachidate (1.411 %) were also detected in the produced biodiesel.

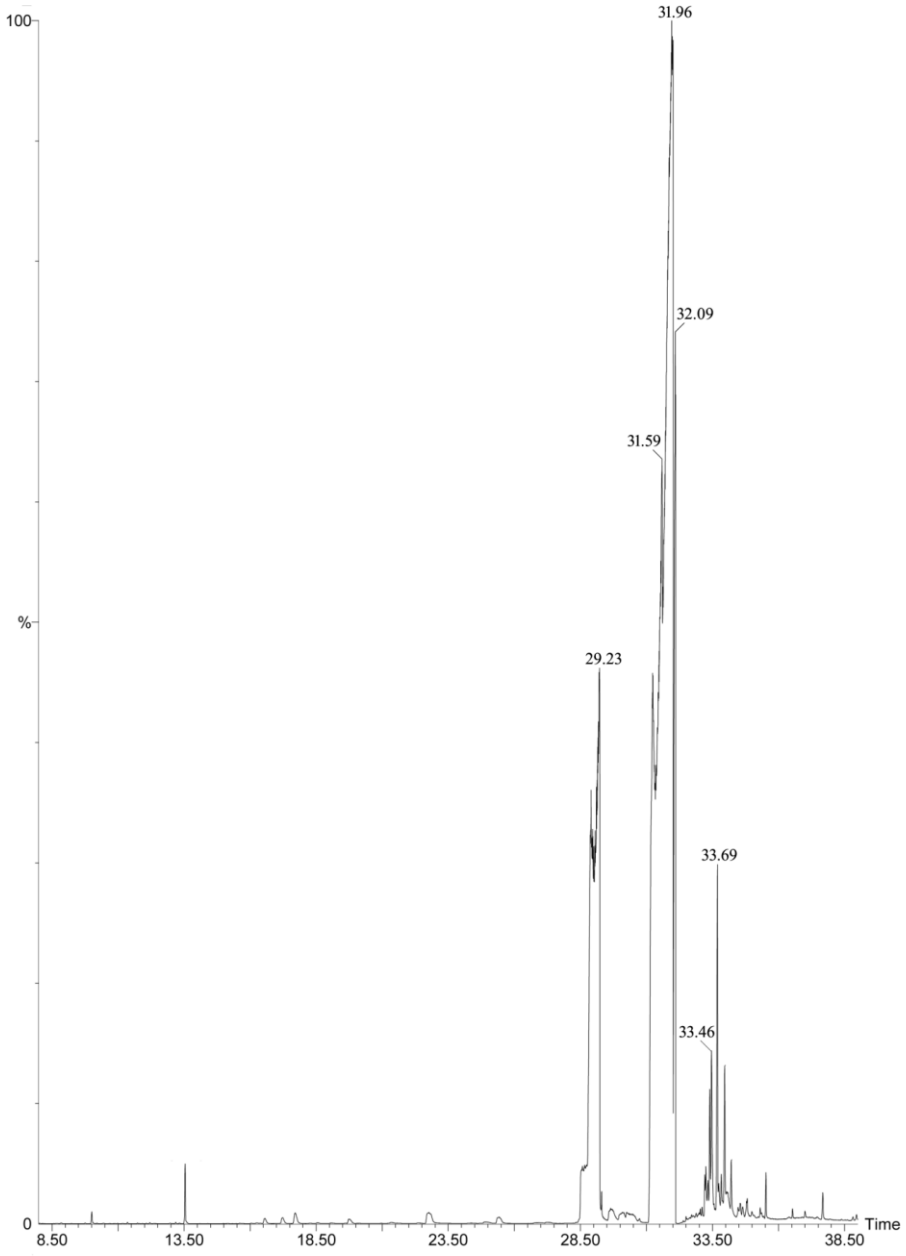

Fig. 3.24. GC chromatogram of jatropha biodiesel.

Table 3.9: Composition of jatropha biodiesel

RT	Methyl esters	Composition (%)
29.23	Methyl palmitate [C16:0]	25.205
31.59	Methyl linoleate [C18:2]	19.518
31.96	Methyl oleate [C18:1]	45.575
32.09	Methyl stearate [C18:0]	6.051
33.46	Methyl gondoate [C20:1]	1.106
33.69	Methyl arachidate [C20:0]	1.411

3.3.5 Biodiesel properties

The physicochemical properties of biodiesel of this work are compared to that of some reported biodiesel fuels produced using the similar type of catalysts are presented in **Table 3.10**. In this study, the acid value (AV) and FFA of *J. curcas* oil was found to be 11.57 mg KOH/g and 5.75 mg KOH/g, respectively. This oil was employed for the synthesis of biodiesel via direct transesterification without any pretreatment or esterification significantly using the prepared solid catalyst. After the transesterification, the AV of produced biodiesel reduced to 0.2035 mg KOH/g (FFA of 0.1017 mg KOH/g) which is within the maximum limit of 0.5 mg KOH/g specified in the EN 14214 standard. Chouhan and Sarma (2013), Taufiq-Yap et al. (2014) and Sudsakorn et al. (2017) reported the AV of *J. curcas* oil as 7.46, 13.60 and 5.974 mg KOH/g, respectively. They directly transesterified *J. curcas* oil into biodiesel successfully without pretreatment by employing heterogeneous base catalysts. *Mesua ferrea* oil with AV of 18.8 mg KOH/g was also transesterified directly using heterogeneous base catalyst derived from *Musa balbisiana* stem (Aslam et al., 2014). In this study, the AV of biodiesel was found to be similar to that of the reported data (Daimary et al., 2022a; Falowo and Betiku, 2022). The low acid value of biodiesel does not cause sediment formation or corrosion in fuel systems (Olatundun et al., 2020). In this work, the specific gravity of biodiesel fuels was found to be 0.8797 which satisfies the limit (0.86–0.90) prescribed by ASTM D6751. The density of biodiesel at 15 ^{o}C was determined to be 0.877 g cm^{-3} and is within the range of EN 14214 (0.86-0.90 g cm^{-3}) and ASTM D6751 (0.86-0.90 g cm^{-3}) standards. This implies that a fuel is suitable for combustion and good atomization. In other respect, a heavier fuel density produces lower volatility and poor atomization during fuel injection, resulting incomplete combustion

and carbon deposits inside the combustion chamber (Yahya et al., 2018). The kinematic viscosity of *J. curcas* biodiesel at 40 ^{o}C was 4.136 $mm^2 s^{-1}$, which is within the standard limits and this is comparatively lower than the reported biodiesel fuels by Changmai et al. (2020b) and Rajkumari and Rokhum (2020). However, Daimary et al. (2022a), Foroutan et al. (2022), Gohain et al. (2020b), Nath et al. (2019; 2020) reported slightly lower kinematic viscosity values. It is reported that higher kinematic viscosity of fuel leads to poor atomization due to the formation of a larger droplet on injection into the engine which occurs incomplete combustion and carbon deposition (Benni et al., 2021). On the other hand, the too-low viscosity of fuel also causes leakage or tears in the fuel pump due to inadequate lubrication (Benni et al., 2021). The cetane number of the biodiesel was 48.1, which is comparatively close to the recommended (minimum 47 and 51) standard values. Thus, the produced biodiesel in this work has a capability to ignite without delay (Olatundun et al., 2020). The cetane index of present biodiesel was computed as 54.234. The calculated saponification number (SN) for the present biodiesel was 191.39 mg KOH/g which is well-comparable with SN for the other reported biodiesel fuels (Nath et al., 2019; Nath et al., 2020). The obtained SN expressed the agreeable specification of biodiesel because it indicates normal constituents of fatty acids. Due to the fact that the oil or biodiesel with a high SN have a higher percentage of low molecular weight fatty acids (Barua et al., 2014; Ismail and Ali, 2015). The iodine value of biodiesel is an essential specification that indicates the unsaturation level in the oil or fat. Biodiesel with a low iodine value is usually advantageous (Diwakar et al., 2010). The obtained iodine value for the present biodiesel was 73.70 g I_2/100 g, and this is a favorable value and far below the maximum value (120 g I_2/100 g) as prescribed in EN 14214 standard. In this study, the other fuel properties such as cold filter plugging point (^{o}C), diesel index, API and aniline point were determined to be <4, 66.99, 34.27, and 195.44, respectively. The empirically calculated HHV of present biodiesel was 40.47 MJ/kg, indicating the sufficient quantity required for the release of heat for the whole combustion of 1 kg of biodiesel. That means the synthesized biodiesel has an adequate calorific value to substitute petrodiesel as a clean fuel (Oladipo et al., 2020). The HHV of present biodiesel is comparable with the HHV of other biodiesel fuels (**Table 3.10**) reported by Gohain et al. (2017; 2020b), Changmai et al. (2020b), Falowo and Betiku (2022), Nath et al. (2019) and Daimary et al. (2022a).

Table 3.10: Properties of jatropha biodiesel and comparison with standards and reported biodiesels.

Properties	**Jatropha biodiesel (This work)**	**ASTM D6751**	**EN 14214**	**Reported biodiesels**								
				Yellow oleander-rubber oil (Falowo and Betiku, 2022)	**WCO** (Daimary et al., 2022a)	**WCO** (Gohain et al., 2020b)	**Soybean oil** (Changmai et al., 2020a)	**Soybean oil** (Rajkumari and Rokhum, 2020)	***Moringa oleifera* oil** (Foroutan et al., 2022)	**WCO** (Gohain et al., 2017)	**Sunflower oil** (Nath et al., 2020)	**Soybean oil** (Nath et al., 2019)
Density at 15 ^{o}C (g/cm^3)	0.877	0.86–0.90	0.86–0.90	0.887	0.88	0.85	0.86	0.872	0.874	0.89	0.859	0.8606
Specific gravity	0.8797	0.86–0.90	-	-	-	-	-	-	-	-	0.854	0.8615
Kinematic viscosity at 40 ^{o}C (mm^2/s)	4.136	1.9–6.0	3.5–5.0	-	3.90	-	5.88	5.42	4.1	3.12	3.11	3.76
Cetane number	48.1	47 (min)	51 (min)	55	52	58	51	-	55.56	55	53.95	56.67
Cetane index	54.234	NS	NS	-	-	-	-	-	-	-	-	56.13
Pour point (^{o}C)	0	NS	NS	-	-6	-9	−0.2		-1	-9	-6	-3

CFPP (°C)	<4	NS	NS	-	-	-	-	-	-	-	-3	0
SN (mg KOH/g)	191.39	NS	NS	-	-	-	-	-	-	-	188.57	176.33
Iodine value (g I_2/100 g)	73.70	NS	120 (max)	75.65	-	-	-	-	-	-	-	121.91
API	34.27	36.95	NS	-	-	-	-	-	-	-	34.277	32.756
Diesel index	66.99	50.4	NS	-	-	-	-	-	-	-	50.82	55.309
Aniline point	195.44	331	-	-	-	-	-	-	-	-	148.27	168.85
HHV (MJ/kg)	40.47	NS	NS	39.70	39.80	39.32	38.2	-	-	40.20	39.79	40.37

WCO–Waste cooking oil; NS–Not specified; max– maximum; min– minimum; CFPP–Cold filter plugging point; SN–Saponification number; API–American petroleum index; HHV–Higher heating value.

3.4 Conclusion

In conclusion, it can be summarized that biodiesel production from *J. curcas* oil was successful with the application of post-harvest *M. champa* plant derived different materials such as BMCP, BMCS, BMCR, CMCP-550, CMCS-550, and CMCR-550 catalysts. At the ORCs (9:1 MTOMR, 5 wt. %, 65 ^{o}C), the catalytic efficacies demonstrated was in the order of CMCP-550 (98.27 %, 10 min) > CMCR-550 (97.89 %, 14 min) > CMCS-550 (97.78 %, 60 min). This trend was because of the basicity of the catalyst which was in the similar order of CMCP-550 (1.25 mmol g^{-1}) > CMCR-550 (0.91 mmol g^{-1}) > CMCS-550 (0.42 mmol g^{-1}) and their basic character was mostly due to K contents present in the catalysts. The catalytic activities of the *M. champa* burnt ash catalysts were found in the order of BMCP > BMCR > BMCS, the best one being the BMCP catalyst that produced a high yield of 96.70 % biodiesel in 45 min at the same ORCs. This trend was also in good agreement with the K contents of the burnt ash catalysts. In this study, the CMCP-550 catalyst with a surface area of 6.848 m^2 g^{-1} and micro-mesoporous structure is showing the best and superior efficacy among the different calcined and burnt ash catalysts. This is because of its stronger basicity, which was accredited due to its higher quantity of K that existed as K_2CO_3 and K_2O. The CMCP-550 catalyzed reaction exhibited an activation energy of 54.256 kJ mol^{-1} with a TOF of 14.15 h^{-1}. The CMCP-550 catalyst showed a gradual decrease in catalyst reusability test with a biodiesel yield of 93.79 % in the 3rd cycle. The catalysts from post-harvest *M. champa* plant are inexpensive, inexhaustible, easily derivable, reusable, non-toxic, environmentally friendly, and labor-efficient, and consequently, can be potentially used as the cost-effective catalyst for low-cost biodiesel production at large-scale."